Novel pseudomomentum-translational sum rule for the molecular Berry curvature

Dominik Steinmetz[1] and Ansgar Pausch*[2]
[1)]*Institute of Physical Chemistry, Karlsruhe Institute of Technology (KIT), Fritz-Haber-Weg 2, 76131 Karlsruhe, Germany*
[2)]*Theoretical Chemistry, Vrije Universiteit Amsterdam, 1081HV Amsterdam, The Netherlands*

(*Email for correspondence: a.i.pausch@vu.nl)

(Dated: 30 January 2025)

The molecular Berry curvature plays an important role for electronic structure calculations within the adiabatic Born–Oppenheimer approximation and is connected to many magnetic phenomena such as the Aharanov–Bohm and the chirality-induced spin selectivity (CISS) effect. For molecules in external magnetic fields, the Berry curvature is essential to achieve a qualitatively correct description of nuclear motion. Here, it is responsible for screening the Lorentz forces acting on moving nuclear charges. This connection has recently been exploited to derive a new type of population analysis known as Berry charges. In this work, we derive a novel sum rule for the molecular Berry curvature. This *pseudomomentum-translational sum rule* is then used to reveal the connection between Berry charges and the well-known generalized atomic polar tensor (GAPT) charges. Furthermore, we present an efficient integral-direct implementation of the molecular Berry curvature for molecules in finite magnetic fields into the TURBOMOLE program suite. This is used to further demonstrate the connection between Berry and GAPT charges for a variety of larger molecules, comparing the results to other established types of partial charges.

I. INTRODUCTION

The molecular Berry curvature is an important quantity within the adiabatic limit of the Born–Oppenheimer approximation. It may best be understood as a vector field induced by a non-trivial geometric phase of the wave function, which is also often referred to as the Berry phase.[1–3] Both the Berry phase and the Berry curvature contain information about the topology of a system and are linked to many important phenomena such as conical intersections, rotational g-factors, as well as the Aharanov–Bohm and the chirality-induced spin selectivity (CISS) effects.[4–11]

One of the sources for a non-trivial geometric phase of the wave function may be an external magnetic field.[12–17] The resulting Berry curvature leads to an additional velocity-dependent force in the nuclear equations of motion.[18,19] The effects of this so-called Berry force on molecular rotations and vibrations have recently been studied with molecular dynamics, in the harmonic limit, and with time-dependent nuclear-electronic orbital Hartree–Fock theory.[20–23] Due to the intuitive connection between the Berry force and corresponding Lorenz forces, it was also noted that the Berry curvature allows for the definition of an effective nuclear charge which may be used to define a new type of population analysis.[24] The partial charges obtained from this method are known as Berry charges.

Both a numerical and an analytical approach have been proposed for the calculation of the molecular Berry curvature in an external magnetic field.[18,25,26] The numerical approach is limited in its numerical accuracy and it requires a somewhat tedious scheme to eliminate any dependency on the global phase of the wave function.[18,25] While the analytical approach does not suffer from these problems, it requires the solution of linear response equations, a step which formally scales as $\mathcal{O}(N^5)$.[26] It should be noted that both of these approaches are associated with similarly high computational cost.

As an alternative, the molecular Berry curvature may also be approximated using its connection to effective nuclear charges.[27] For this, some flavor of population analysis is computed for the molecular system – this may be Mulliken,[28–30] Löwdin,[31] Bader,[32] or Hirshfeld charges,[33] partial charges obtained from an electrostatic potential fit based on the Kollman parametrization,[34] or any other type of effective nuclear charge. These are then combined to approximate the molecular Berry curvature, constraint by the properties we wish to preserve. This includes, most importantly, the antisymmetric tensor structure and the magnetic-translational sum rule.[27]

In this work, we introduce a novel translational sum rule for the molecular Berry curvature. This *pseudomomentum-translational sum rule* is an important relation which to the best of our knowledge has not been described in the literature yet. Through this sum rule, a key connection between Berry charges and generalized atomic polar tensor (GAPT) charges[35,36] is revealed. The latter are well-known in literature, which allows for an in-depth discussion about the benefits and limitations of using Berry charges to interpret them in terms of atomic partial charges. In addition to providing this link between methods, the novel sum rule may be used to facilitate the calculation of Berry charges.

To analyze the molecular Berry curvature as well as the pseudomomentum-translational sum rule, we present a highly efficient, analytical implementation into the TURBOMOLE[37–39] program suite. This is based on the integral-direct response algorithm in our spin-noncollinear implementation of the finite field (ff)[40] approach which employs London atomic orbitals (LAOs)[41,42] to ensure gauge

origin invariance.[43–47] Other notable ff-LAO implementations in established quantum chemistry software include those in LONDON,[48,49] ChronusQ,[50–52] QCUMBRE,[53–55] BAGEL,[56,57] and QUEST.[58–60]

The remainder of this work is structured as follows. In section II, we first present a rigorous derivation of the pseudomomentum-translational sum rule. We then reintroduce the concept of the Berry population analysis which was first proposed in Ref. 24. Using the novel sum rule, we demonstrate the close relation between Berry charges and GAPT charges.

Section III introduces our efficient, integral-direct implementation for the calculation of the molecular Berry curvature. Particular emphasis is put on the construction of the perturbed Fock matrix in the coupled perturbed Hartree–Fock (CPHF) equations. We adapt a technique first used for the analytical calculation of geometry Hessians in the absence of magnetic fields, through which a direct transformation of the two-electron integrals into the spinor basis can be avoided.[61,62] This significantly increases the computational efficiency of the algorithm.

In section IV, we provide the computational details for all calculations carried out in the context of this work. Finally, in section V, we analyze the novel pseudomomentum-translational sum rule and investigate its connection to Berry charges for a variety of molecular systems. Berry charges are compared to other types of partial charges and an important connection to the electronic dipole moment is uncovered. We close this section by analyzing the basis set convergence of Berry and GAPT charges, demonstrating that they are equivalent in the limit of a complete basis. This work is then concluded in sec. VI.

II. THEORY

A. Preface and notation

The derivations in this chapter largely follow a previous work presented by Peters, Culpitt, Tellgren, and Helgaker in Ref. 27. Therein, the magnetic-translational sum rule for the molecular Berry curvature is derived in the framework of the adiabatic Born–Oppenheimer approximation.[18,19,25] While the derivation here is specifically carried out for molecular systems in an external magnetic field (**B**), its generality should be heavily emphasized. In the absence of external fields, a Berry curvature may for instance also be induced through relativistic effects such as spin–orbit coupling or through the band structure of solids.[63,64]

We use Hartree atomic units throughout this work if not stated otherwise. Matrix $\mathbf{R}$ contains all nuclear coordinates while the position vector $\mathbf{R}_I$ contains the coordinates of atom I. Electronic coordinates are described through their position vector $\mathbf{r}$. Integration within the bra–ket notation is carried out over the electronic coordinates. Greek indices indicate Cartesian coordinates: $\alpha,\beta,\gamma \in \{x,y,z\}$. The Einstein summation convention is used for repeated Greek indices only. We use δ_{ij} for the Kronecker delta and ε_{ijk} for the Levi–Civita tensor.

B. The molecular Berry curvature

The adiabatic limit of the Born–Oppenheimer approximation gives rise to a geometric vector potential, often also referred to as Berry connection:[1–3]

$$\chi_{I\alpha}(\mathbf{R},\mathbf{O}) = \langle \phi(\mathbf{r},\mathbf{R},\mathbf{O}) | \hat{P}_{I\alpha} \phi(\mathbf{r},\mathbf{R},\mathbf{O}) \rangle \,. \tag{1}$$

It acts as an additional potential in the nuclear Hamiltonian and has similar properties as a vector potential.[12,13,18] As indicated by its dependency on the gauge origin $\mathbf{O}$, it is a gauge-variant quantity. In its definition, it contains the nuclear momentum operator,

$$\hat{P}_{I\alpha} = -\mathrm{i}\nabla_{I\alpha} \,, \tag{2}$$

which is not a Hermitian operator in the Hilbert space spanned by electronic coordinates. Consequently, the integration in eq. (1) yields a complex-valued result and carries a trivial (global) phase. The electronic wave function $|\phi(\mathbf{r},\mathbf{R},\mathbf{O})\rangle$ is taken to be an exact eigenfunction of the electronic Hamiltonian here:

$$\hat{H}^{\mathrm{el}}(\mathbf{r},\mathbf{R},\mathbf{O})\,|\phi(\mathbf{r},\mathbf{R},\mathbf{O})\rangle = E^{\mathrm{el}}(\mathbf{R})\,|\phi(\mathbf{r},\mathbf{R},\mathbf{O})\rangle \,. \tag{3}$$

It should be noted that the electronic Hamiltonian $\hat{H}^{\mathrm{el}}$ is a Hermitian operator acting on the Hilbert space of the electronic wave function. While the electronic Hamiltonian itself is gauge-variant, the electronic energy E^{el} is not.[65] As such, the gauge-dependency of $\hat{H}^{\mathrm{el}}$ is canceled out by the electronic wave function $|\phi(\mathbf{r},\mathbf{R},\mathbf{O})\rangle$. A proper gauge transformation is an important property of the exact wave function which should be retained even by approximate wave functions. This can be ensured by the use of London atomic orbitals.[27,41,42]

The molecular Berry curvature can be obtained from the Berry connection through the following relation:[18]

$$\Omega_{I\alpha,J\beta}(\mathbf{R}) = \frac{\partial \chi_{I\alpha}(\mathbf{R},\mathbf{O})}{\partial R_{J\beta}} - \frac{\partial \chi_{J\beta}(\mathbf{R},\mathbf{O})}{\partial R_{I\alpha}} \,. \tag{4}$$

The molecular Berry curvature is an antisymmetric tensor: $\Omega_{I\alpha,J\beta} = -\Omega_{J\beta,I\alpha}$. By inserting the definition of the Berry connection into eq. (4), we can cast it in another, convenient form:

$$\Omega_{I\alpha,J\beta}(\mathbf{R}) = -2\,\mathrm{Im}\left\langle \frac{\partial \phi(\mathbf{r},\mathbf{R},\mathbf{O})}{\partial R_{I\alpha}} \middle| \frac{\partial \phi(\mathbf{r},\mathbf{R},\mathbf{O})}{\partial R_{J\beta}} \right\rangle . \tag{5}$$

Unlike the geometric vector potential, the Berry curvature is gauge-invariant.[18] This property is retained for all approximate wave functions considered in this work.[27]

C. Translational sum rules

We now introduce two translational sum rules for the molecular Berry curvature. The novel *pseudomomentum-*

translational sum rule,

$$\sum_{J}^{N_{\text{nuc}}} \Omega_{I\alpha,J\beta}(\mathbf{R}) = \frac{\partial k_\beta(\mathbf{R})}{\partial R_{I\alpha}}\,, \tag{6}$$

$$\sum_{I}^{N_{\text{nuc}}} \Omega_{I\alpha,J\beta}(\mathbf{R}) = -\frac{\partial k_\alpha(\mathbf{R})}{\partial R_{J\beta}}\,, \tag{7}$$

relates a summation over one nuclear index of the molecular Berry curvature to a nuclear displacement of the electronic pseudomomentum $\mathbf{k}$ and N_{nuc} refers to the number of nuclei in the molecular system. Eqs. (6) and (7) are related via the antisymmetry of the molecular Berry curvature. The *magnetic-translational sum rule*,

$$\sum_{I,J}^{N_{\text{nuc}}} \Omega_{I\alpha,J\beta}(\mathbf{R}) = N_{\text{el}} \tilde{B}_{\alpha\beta}\,, \tag{8}$$

was discussed in detail in Ref. 27 and relates a summation over both nuclear indices of the molecular Berry curvature to the number of electrons N_{el} and the external magnetic field. The field tensor is defined as $\tilde{B}_{\alpha\beta} = -\varepsilon_{\alpha\beta\gamma}B_\gamma$, which can be written as:

$$\tilde{\mathbf{B}} = \begin{pmatrix} 0 & -B_z & B_y \\ B_z & 0 & -B_x \\ -B_y & B_x & 0 \end{pmatrix}. \tag{9}$$

The validity of both sum rules in eqs. (6) and (8) also automatically implies the existence of another sum rule,

$$\sum_{I}^{N_{\text{nuc}}} \frac{\partial k_\beta(\mathbf{R})}{\partial R_{I\alpha}} = N_{\text{el}} \tilde{B}_{\alpha\beta}\,, \tag{10}$$

which is given here for the sake of completeness. It relates the nuclear displacements of the electronic pseudomomentum to the number of electrons and the external magnetic field. A coordinate of the electronic pseudomomentum is defined by[27]

$$k_\alpha(\mathbf{R}) = \langle \phi(\mathbf{r},\mathbf{R},\mathbf{O}) | \hat{k}_\alpha \phi(\mathbf{r},\mathbf{R},\mathbf{O}) \rangle\,, \tag{11}$$

with the pseudomomentum operator $\hat{\mathbf{k}}$ being constructed from the kinetic momentum operator $\hat{\boldsymbol{\pi}}$, the magnetic field tensor and the position operator $\hat{\mathbf{r}}$. A coordinate can be defined as:[27]

$$\hat{k}_\alpha = \hat{\pi}_\alpha - \tilde{B}_{\alpha\beta}\hat{r}_\beta\,. \tag{12}$$

The kinetic momentum operator is constructed via minimal coupling[66]

$$\hat{\pi}_\alpha = \hat{p}_\alpha + A_\alpha(\mathbf{r},\mathbf{O}) \tag{13}$$

from the canonical momentum operator

$$\hat{p}_\alpha = -\mathrm{i}\nabla_\alpha \tag{14}$$

and the magnetic vector potential

$$A_\alpha(\mathbf{r},\mathbf{O}) = \frac{1}{2}\tilde{B}_{\alpha\beta}(r_\beta - O_\beta)\,, \tag{15}$$

which is cast here in the symmetric gauge, a special case of the Coulomb gauge ($\boldsymbol{\nabla}\cdot\mathbf{A} = 0$) for static, homogeneous magnetic fields. This allows us to write the electronic pseudomomentum operator in a more convenient form, with one of its coordinates being given as:

$$\hat{k}_\alpha = \hat{p}_\alpha - \frac{1}{2}\tilde{B}_{\alpha\beta}(r_\beta + O_\beta)\,. \tag{16}$$

Despite the dependence of the operator $\hat{\mathbf{k}}$ on the gauge origin $\mathbf{O}$, the electronic pseudomomentum $\mathbf{k}(\mathbf{R})$ is gauge origin invariant if the electronic wave function transforms properly under gauge transformations. As previously discussed, this is the case for exact wave functions and for all approximate wave functions considered in this work.[27]

D. Sum rule in the limit of a complete basis

Before presenting a detailed derivation, we now briefly discuss how the pseudomomentum-translational sum rule can be simplified further for wave functions in the limit of a complete basis. Using the definition of the electronic pseudomomentum and its operator in eqs. (11) and (16), respectively, we can reframe the pseudomomentum-translational sum rule as:

$$\sum_{J}^{N_{\text{nuc}}} \Omega_{I\alpha,J\beta}(\mathbf{R}) = \frac{\partial p_\beta(\mathbf{R},\mathbf{O})}{\partial R_{I\alpha}} + \frac{1}{2}\tilde{B}_{\beta\gamma}\frac{\partial \mu_\gamma(\mathbf{R},\mathbf{O})}{\partial R_{I\alpha}}\,. \tag{17}$$

Here, we have introduced the electronic canonical momentum $\mathbf{p}$ and the electronic dipole moment $\boldsymbol{\mu}$, respectively:

$$p_\alpha(\mathbf{R},\mathbf{O}) = \langle \phi(\mathbf{r},\mathbf{R},\mathbf{O}) | \hat{p}_\alpha \phi(\mathbf{r},\mathbf{R},\mathbf{O}) \rangle\,; \tag{18}$$

$$\mu_\alpha(\mathbf{R},\mathbf{O}) = -\langle \phi(\mathbf{r},\mathbf{R},\mathbf{O}) | (\hat{r}_\alpha - O_\alpha) \phi(\mathbf{r},\mathbf{R},\mathbf{O}) \rangle\,. \tag{19}$$

Similarly, a coordinate of the electronic kinetic momentum $\boldsymbol{\pi}$ can be defined as

$$\pi_\alpha(\mathbf{R}) = \langle \phi(\mathbf{r},\mathbf{R},\mathbf{O}) | \hat{\pi}_\alpha \phi(\mathbf{r},\mathbf{R},\mathbf{O}) \rangle\,, \tag{20}$$

and it can be interpreted as the general motion of electrons in the molecular system. Evidently, bound electrons in a molecule should not experience an overall kinetic momentum and they should satisfy the continuity equation.[67,68] For electronic ground states, this condition implies that:

$$\boldsymbol{\pi} = 0\,. \tag{21}$$

Using the original definition of the electronic pseudomomentum operator in eq. (12), we can write:

$$k_\alpha = \pi_\alpha + \tilde{B}_{\alpha\beta}\mu_\beta\,. \tag{22}$$

For exact wave functions, this then simplifies to

$$k_\alpha = \tilde{B}_{\alpha\beta}\mu_\beta \tag{23}$$

and the corresponding sum rule becomes:

$$\sum_{J}^{N_{\text{nuc}}} \Omega_{I\alpha,J\beta}(\mathbf{R}) = \tilde{B}_{\beta\gamma}\frac{\partial \mu_\gamma(\mathbf{R},\mathbf{O})}{\partial R_{I\alpha}}\,. \tag{24}$$

This relation, however, holds only for wave functions in a complete basis. For any wave function expanded in an incomplete basis, the condition in eq. (21) is no longer necessarily satisfied. This can be understood by examining the two components of the electronic kinetic momentum operator:

$$\hat{\pi}_\alpha = \hat{p}_\alpha + \frac{1}{2}\tilde{B}_{\alpha\beta}(\hat{r}_\beta - O_\beta)\,. \tag{25}$$

While the position operator $\hat{\mathbf{r}}$ has an exact representation in coordinate space, the momentum operator $\hat{\mathbf{p}}$ has one in momentum space. The two are related through a Fourier transformation, which is exact only in the limit of a complete basis. As such, the gauge-dependency of the electronic canonical momentum $\mathbf{p}(\mathbf{R},\mathbf{O})$ and that of the electronic dipole moment $\boldsymbol{\mu}(\mathbf{R},\mathbf{O})$ will generally not cancel for a wave function in an incomplete basis.

E. Derivation of the pseudomomentum-translational sum rule

We now present a detailed derivation of the novel pseudomomentum-translational sum rule, thereby proving its validity. The derivation presented here follows in large parts the one presented for the magnetic-translational sum rule by Peters, Culpitt, Tellgren, and Helgaker in Ref. 27 and is thus held a bit more concise here. The interested reader is referred to that work for any additional information.

We begin this derivation by considering the summation of the molecular Berry curvature over one nuclear index in eq. (4):

$$\sum_J^{N_\mathrm{nuc}} \Omega_{I\alpha,J\beta}(\mathbf{R}) = \sum_J^{N_\mathrm{nuc}} \frac{\partial}{\partial R_{J\beta}}\chi_{I\alpha}(\mathbf{R},\mathbf{O}) - \frac{\partial}{\partial R_{I\alpha}}\sum_J^{N_\mathrm{nuc}} \chi_{J\beta}(\mathbf{R},\mathbf{O})\,. \tag{26}$$

In order to rearrange the first term in eq. (26), we define a translation of all nuclear coordinates of the system by some displacement vector $\mathbf{T}$, which leaves both the electronic coordinates and the gauge origin unchanged:[27]

$$\mathbf{R} + \mathbf{R}_\mathrm{T} = \begin{pmatrix} \mathbf{R}_1 + \mathbf{T} \\ \mathbf{R}_2 + \mathbf{T} \\ \vdots \end{pmatrix}\,. \tag{27}$$

Here, we note that a displacement of all nuclear coordinates is equivalent to a translation of all atoms, which allows us to rewrite the sum of all nuclear derivative operators as:

$$\frac{\partial}{\partial T_\beta} = \sum_J \frac{\partial}{\partial R_{J\beta}}\,. \tag{28}$$

For the second term in eq. (26), we define the sum of all nuclear canonical momentum terms as the total nuclear canonical momentum of the system:[27]

$$\sum_J^{N_\mathrm{nuc}} \hat{P}_{J\beta} = \hat{P}^\mathrm{tot}_\beta\,. \tag{29}$$

Inserting eqs. (28) and (29) into eq. (26) yields:

$$\sum_J^{N_\mathrm{nuc}} \Omega_{I\alpha,J\beta} = \frac{\partial}{\partial T_\beta}\langle\phi|\hat{P}_{I\alpha}\phi\rangle - \frac{\partial}{\partial R_{I\alpha}}\langle\phi|\hat{P}^\mathrm{tot}_\beta\phi\rangle\,, \tag{30}$$

which reframes the summation over the molecular Berry curvature in terms of a translation of an individual nuclear canonical momentum and a nuclear displacement of the total nuclear canonical momentum. We have omitted the arguments of $\phi(\mathbf{r},\mathbf{R},\mathbf{O})$ in eq. (30) for the sake of brevity.

We will now derive a concrete form for the total nuclear canonical momentum operator $\hat{\mathbf{P}}^\mathrm{tot}$. For this, we need to consider the effects of a translation of all nuclear coordinates on the system and finally evaluate this in the limit of a vanishing translation ($\mathbf{T}\to\mathbf{0}$). We begin with considering how the electronic Hamiltonian transforms if all nuclear coordinates are translated by $\mathbf{T}$. The transformed Hamiltonian may be obtained through a unitary transformation,

$$\hat{H}^\mathrm{el}(\mathbf{r},\mathbf{R}+\mathbf{R}_\mathrm{T},\mathbf{O}) = \hat{U}(\mathbf{R},\mathbf{T},\mathbf{O})\hat{H}^\mathrm{el}(\mathbf{r},\mathbf{R},\mathbf{O})\hat{U}^\dagger(\mathbf{R},\mathbf{T},\mathbf{O})\,, \tag{31}$$

and the corresponding electronic wave function transforms accordingly:

$$|\phi(\mathbf{r},\mathbf{R}+\mathbf{R}_\mathrm{T},\mathbf{O})\rangle = \hat{U}(\mathbf{R},\mathbf{T},\mathbf{O})\,|\phi(\mathbf{r},\mathbf{R},\mathbf{O})\rangle\,. \tag{32}$$

This unitary transformation operator contains a non-trivial phase induced by the translation, which is directly connected to the electronic pseudomomentum operator $\hat{\mathbf{k}}$. In addition, it contains a trivial phase, which consists of an arbitrary gauge function $\eta(\mathbf{R},\mathbf{T},\mathbf{O})$. The unitary transformation operator can be written as:[27]

$$\hat{U}(\mathbf{R},\mathbf{T},\mathbf{O}) = \exp\big(-\mathrm{i}\,\mathbf{T}\cdot\hat{\mathbf{k}} + \mathrm{i}\eta(\mathbf{R},\mathbf{T},\mathbf{O})\big)\,. \tag{33}$$

Please note that eqs. (31)–(33) hold true for any choice of gauge origin. Hence we will omit $\mathbf{O}$ for the sake of brevity from now on. Next, we apply the translation to the total nuclear momentum operator:

$$\hat{P}^{\mathrm{U,tot}}_\alpha(\mathbf{R},\mathbf{T}) = \hat{U}^\dagger(\mathbf{R},\mathbf{T})\,\hat{P}^\mathrm{tot}_\alpha\,\hat{U}(\mathbf{R},\mathbf{T})\,. \tag{34}$$

By evaluating a Baker–Campbell–Hausdorff expansion in which all third and higher order terms vanish, one obtains:[27]

$$\hat{P}^{\mathrm{U,tot}}_\alpha(\mathbf{R},\mathbf{T}) = -\mathrm{i}\frac{\partial}{\partial T_\alpha} - \hat{k}_\alpha + \hat{\gamma}_\alpha(\mathbf{R},\mathbf{T}) + \frac{1}{2}N_\mathrm{el}\tilde{B}_{\alpha\beta}T_\beta\,. \tag{35}$$

Here, $\hat{\gamma}$ is the derivative of the gauge function with respect to $\mathbf{T}$,

$$\hat{\gamma}_\alpha(\mathbf{R},\mathbf{T}) = \frac{\partial\eta(\mathbf{R},\mathbf{T})}{\partial T_\alpha}\,, \tag{36}$$

which is real-valued because $\eta(\mathbf{R},\mathbf{T})$ is also real-valued by construction. If we now consider the effect of the total nuclear momentum operator on the wave function of a displaced reference system, we obtain:

$$\hat{P}^\mathrm{tot}_\alpha\,|\phi(\mathbf{r},\mathbf{R}+\mathbf{R}_\mathrm{T})\rangle = \hat{P}^\mathrm{tot}_\alpha\hat{U}(\mathbf{R},\mathbf{T})\,|\phi(\mathbf{r},\mathbf{R})\rangle \tag{37}$$

$$= \hat{U}(\mathbf{R},\mathbf{T})\hat{P}^{\mathrm{U,tot}}_\alpha(\mathbf{R},\mathbf{T})\,|\phi(\mathbf{r},\mathbf{R})\rangle\,. \tag{38}$$

By evaluating eq. (37) at $\mathbf{T} = 0$, we finally obtain an expression for the total nuclear momentum operator at vanishing displacement of the nuclear coordinates:

$$\hat{P}_\alpha^{\text{tot}} |\phi(\mathbf{r},\mathbf{R})\rangle = (\hat{\gamma}_\alpha(\mathbf{R}) - \hat{k}_\alpha) |\phi(\mathbf{r},\mathbf{R})\rangle \,. \tag{39}$$

We can insert eq. (39) into our sum rule in (30) and we may additionally use the fact that $\hat{\gamma}(\mathbf{R})$ is not dependent on the electronic coordinate,

$$\gamma_\alpha(\mathbf{R}) = \langle \phi(\mathbf{r},\mathbf{R}) | \hat{\gamma}_\alpha(\mathbf{R}) \phi(\mathbf{r},\mathbf{R}) \rangle \,, \tag{40}$$

to arrive at the following expression for the sum rule:

$$\sum_J^{N_{\text{nuc}}} \Omega_{I\alpha,J\beta} = \frac{\partial}{\partial T_\beta} \langle \phi | \hat{P}_{I\alpha} \phi \rangle - \frac{\partial \gamma_\beta(\mathbf{R})}{\partial R_{I\alpha}} + \frac{\partial k_\beta(\mathbf{R})}{\partial R_{I\alpha}} \,. \tag{41}$$

By comparing the sum rule in eq. (41) to its final form given in eq. (6), we realize that we only have to demonstrate that

$$\frac{\partial}{\partial T_\beta} \langle \phi | \hat{P}_{I\alpha} \phi \rangle = \frac{\partial \gamma_\beta(\mathbf{R})}{\partial R_{I\alpha}} \tag{42}$$

holds true. In other words, we have to show that the translation of the Berry connection may at most result in the displacement of the gauge function. Intuitively, this sounds very reasonable considering that the Berry connection is often interpreted as a vector potential.[12,13,18] We shall now demonstrate that the relation presented in eq. (42) indeed holds true and thereby proof the validity of the pseudomomentum-translational sum rule. We use the product rule of derivatives to rewrite the expression as:

$$\frac{\partial}{\partial T_\beta} \langle \phi | \hat{P}_{I\alpha} \phi \rangle = \left\langle \frac{\partial \phi}{\partial T_\beta} \middle| -\mathrm{i} \frac{\partial \phi}{\partial R_{I\alpha}} \right\rangle + \left\langle \phi \middle| -\mathrm{i} \frac{\partial^2 \phi}{\partial T_\beta R_{I\alpha}} \right\rangle \tag{43}$$

$$= \left\langle -\left(\mathrm{i} \frac{\partial \phi}{\partial T_\beta} \right) \middle| \frac{\partial \phi}{\partial R_{I\alpha}} \right\rangle + \left\langle \phi \middle| \frac{\partial}{\partial R_{I\alpha}} \left(-\mathrm{i} \frac{\partial \phi}{\partial T_\beta} \right) \right\rangle \tag{44}$$

$$= -\left\langle \hat{P}_\beta^{\text{tot}} \phi \middle| \frac{\partial \phi}{\partial R_{I\alpha}} \right\rangle + \left\langle \phi \middle| \frac{\partial}{\partial R_{I\alpha}} \hat{P}_\beta^{\text{tot}} \phi \right\rangle . \tag{45}$$

Please note that we have used Schwarz's theorem to get from eq. (43) to (44). Furthermore, due to the hermicity of both $\hat{\gamma}$ and $\hat{\mathbf{k}}$, we may use the turnover rule and write:

$$\begin{aligned} \frac{\partial}{\partial T_\beta} \langle \phi | \hat{P}_{I\alpha} \phi \rangle = &- \left\langle \phi \middle| (\gamma_\beta(\mathbf{R}) - \hat{k}_\beta) \frac{\partial \phi}{\partial R_{I\alpha}} \right\rangle \\ &+ \left\langle \phi \middle| \frac{\partial}{\partial R_{I\alpha}} (\gamma_\beta(\mathbf{R}) - \hat{k}_\beta) \phi \right\rangle . \end{aligned} \tag{46}$$

Since the electronic pseudomomentum operator $\hat{\mathbf{k}}$ does not dependent on nuclear coordinates, it commutes with any nuclear displacement operator, $[\nabla_{I\alpha}, \hat{k}_\beta] = 0$ and we thus obtain the following relation:

$$\begin{aligned} \left\langle \phi \middle| \frac{\partial}{\partial R_{I\alpha}} (\gamma_\beta(\mathbf{R}) - \hat{k}_\beta) \phi \right\rangle = &\left\langle \phi \middle| (\gamma_\beta(\mathbf{R}) - \hat{k}_\beta) \frac{\partial \phi}{\partial R_{I\alpha}} \right\rangle \\ &+ \frac{\partial \gamma_\beta(\mathbf{R})}{\partial R_{I\alpha}} \end{aligned} \tag{47}$$

Inserting eqs. (46) and (47) into the sum rule presented in eq. (41), we finally arrive at

$$\sum_J^{N_{\text{nuc}}} \Omega_{I\alpha,J\beta}(\mathbf{R}) = \frac{\partial \gamma_\beta(\mathbf{R})}{\partial R_{I\alpha}} - \frac{\partial \gamma_\beta(\mathbf{R})}{\partial R_{I\alpha}} + \frac{\partial k_\beta(\mathbf{R})}{\partial R_{I\alpha}} \,; \tag{48}$$

$$= \frac{\partial k_\beta(\mathbf{R})}{\partial R_{I\alpha}} \tag{49}$$

which is the pseudomomentum-translational sum rule. Please note that while we have assumed $|\phi\rangle$ to be an exact wave function here, the only property which was required is that it transforms according to eq. (32) upon translation of nuclear coordinates. As previously mentioned, it can be shown that this property remains intact for approximate wave functions that are expanded in a basis of LAOs.[27]

F. Berry population analysis

The intuitive connection between the molecular Berry curvature and effective charges has been explored excessively in recent literature.[20–25] In Ref. 24, the concept of a population analysis based on the Berry curvature was discussed in more detail. Here, we focus on the definition of isotropic charges based on the molecular Berry curvature in the limit of a vanishing magnetic field. First, we define the following atomic pseudomomentum tensor which corresponds directly to our novel translational sum rule,

$$\omega_{I,\alpha\beta}(\mathbf{R},\mathbf{B}) = \sum_J^{N_{\text{nuc}}} \Omega_{I\alpha,J\beta}(\mathbf{R},\mathbf{B}) = \frac{\partial k_\beta(\mathbf{R},\mathbf{B})}{\partial R_{I\alpha}} \,, \tag{50}$$

in which we also highlight the explicit dependence on the external field. Without loss of generality, we may assume the magnetic field to be parallel to one of the Cartesian axes in our calculations. We may then obtain the following definition for field-dependent Berry charges,

$$q_I^{x,\text{Berry}}(\mathbf{R},\mathbf{B})\, B_x = 0.5[\omega_{I,yz}(\mathbf{R},\mathbf{B}) - \omega_{I,zy}(\mathbf{R},\mathbf{B})] \,; \tag{51}$$

$$q_I^{y,\text{Berry}}(\mathbf{R},\mathbf{B})\, B_y = 0.5[\omega_{I,zx}(\mathbf{R},\mathbf{B}) - \omega_{I,xz}(\mathbf{R},\mathbf{B})] \,; \tag{52}$$

$$q_I^{z,\text{Berry}}(\mathbf{R},\mathbf{B})\, B_z = 0.5[\omega_{I,xy}(\mathbf{R},\mathbf{B}) - \omega_{I,yx}(\mathbf{R},\mathbf{B})] \,, \tag{53}$$

which directly relates them to the antisymmetric part of the atomic pseudomomentum tensor.[24,25] Please note that Ref. 24 introduces two different charge approximations based on the molecular Berry curvature. In addition to partial charges based on the antisymmetric part of the atomic pseudomomentum tensor (B1), the authors propose a population analysis based on the full tensor (B2).[24] We will limit our discussion here to the former type of population analysis.

In a finite magnetic field, the electronic structure is dependent on the direction of the magnetic field and thus, we also expect the partial charges $q_I^{x,\text{Berry}}$, $q_I^{y,\text{Berry}}$, and $q_I^{z,\text{Berry}}$ to be different. In the limit of a vanishing field, we expect these Berry charges

to converge:

$$q_I^{x,\mathrm{Berry}}(\mathbf{R}) = \lim_{|\mathbf{B}|\to 0} q_I^{x,\mathrm{Berry}}(\mathbf{R},\mathbf{B})\,; \tag{54}$$

$$q_I^{y,\mathrm{Berry}}(\mathbf{R}) = \lim_{|\mathbf{B}|\to 0} q_I^{y,\mathrm{Berry}}(\mathbf{R},\mathbf{B})\,; \tag{55}$$

$$q_I^{z,\mathrm{Berry}}(\mathbf{R}) = \lim_{|\mathbf{B}|\to 0} q_I^{z,\mathrm{Berry}}(\mathbf{R},\mathbf{B})\,. \tag{56}$$

Furthermore, this limit should be independent on the direction of the vanishing field. However, while the Berry charges indeed rapidly converge with a decreasing magnetic field, we generally obtain $q_I^x(\mathbf{R}) \neq q_I^y(\mathbf{R}) \neq q_I^z(\mathbf{R})$, except for a few special cases. In contrast, the isotropic average of these Berry charges always remains invariant with respect to rotations of the field axis:[24,25]

$$\langle q_I^{\mathrm{Berry}}(\mathbf{R})\rangle_{\mathrm{rot}} = \frac{1}{3}\left[q_I^{x,\mathrm{Berry}}(\mathbf{R}) + q_I^{y,\mathrm{Berry}}(\mathbf{R}) + q_I^{z,\mathrm{Berry}}(\mathbf{R})\right]. \tag{57}$$

G. Connection to atomic polar tensors

In Ref. 24, the authors note a striking similarity between Berry charges and those obtained from the atomic polar tensor (APT). Without the pseudomomentum-translational sum rule, however, this connection remained somewhat empirical in nature. In this section, we demonstrate the exact connection between Berry charges and GAPT charges. While the atomic polar tensor is generally defined as the geometry gradient of the molecular dipole moment, we will only focus on the electronic part of this quantity,

$$T_{I,\alpha\beta} = \frac{\partial \mu_\beta}{\partial R_{I\alpha}}\,, \tag{58}$$

in the remainder of this work in order to facilitate the comparison to the Berry population analysis. Direction-dependent charges may be identified as the diagonal elements of the APT:

$$q_I^{x,\mathrm{APT}}(\mathbf{R}) = T_{I,xx}\,; \tag{59}$$

$$q_I^{y,\mathrm{APT}}(\mathbf{R}) = T_{I,yy}\,; \tag{60}$$

$$q_I^{z,\mathrm{APT}}(\mathbf{R}) = T_{I,zz}\,. \tag{61}$$

The rotationally invariant GAPT charges are then obtained as the average of these APT charges:

$$q_I^{\mathrm{GAPT}}(\mathbf{R}) \coloneqq \langle q_I^{\mathrm{APT}}(\mathbf{R})\rangle_{\mathrm{rot}} = \frac{1}{3}\left[T_{I,xx} + T_{I,yy} + T_{I,zz}\right] \tag{62}$$

$$= \frac{1}{3}\left[q_I^{x,\mathrm{APT}}(\mathbf{R}) + q_I^{y,\mathrm{APT}}(\mathbf{R}) + q_I^{z,\mathrm{APT}}(\mathbf{R})\right]. \tag{63}$$

Please note the similarity between eqs. (57) and (62). We will now derive an explicit relation between the two sets of partial charges from the definition of the pseudomomentum-translational sum rule in eq. (17). First, we assume the magnetic field to be parallel to the Cartesian z-axis and formulate an expression for $\boldsymbol{\omega}_I$ which depends explicitly on the electronic dipole moment:

$$\omega_{I,xy} = \frac{\partial k_y}{\partial R_{Ix}} = \frac{\partial p_y}{\partial R_{Ix}} + \frac{B_z}{2}\frac{\partial \mu_x}{\partial R_{Ix}} \tag{64}$$

$$\omega_{I,yx} = \frac{\partial k_x}{\partial R_{Iy}} = \frac{\partial p_x}{\partial R_{Iy}} - \frac{B_z}{2}\frac{\partial \mu_y}{\partial R_{Iy}} \tag{65}$$

Here, we have omitted the explicit dependencies on $\mathbf{R}$ and $\mathbf{O}$ for the sake of brevity. An explicit expression for the corresponding Berry partial charge may now be obtained using eq. (53), which yields:

$$q_I^{z,\mathrm{Berry}} = \frac{1}{2B_z}\left(\frac{\partial p_y}{\partial R_{Ix}} - \frac{\partial p_x}{\partial R_{Iy}}\right) + \frac{1}{4}\left(T_{I,xx} + T_{I,yy}\right). \tag{66}$$

Analogous expressions can be found for the Berry charges $q_I^{x,\mathrm{Berry}}$ and $q_I^{y,\mathrm{Berry}}$, respectively. The isotropic average of Berry charge may then be identified as:

$$\begin{aligned}\langle q_I^{\mathrm{Berry}}\rangle_{\mathrm{rot}} =& \frac{1}{6B_x}\left(\frac{\partial p_z}{\partial R_{Iy}} - \frac{\partial p_y}{\partial R_{Iz}}\right)\\ &+\frac{1}{6B_y}\left(\frac{\partial p_x}{\partial R_{Iz}} - \frac{\partial p_z}{\partial R_{Ix}}\right)\\ &+\frac{1}{6B_z}\left(\frac{\partial p_y}{\partial R_{Ix}} - \frac{\partial p_x}{\partial R_{Iy}}\right)\\ &+\frac{1}{6}\left(T_{I,xx} + T_{I,yy} + T_{I,zz}\right).\end{aligned} \tag{67}$$

Since we use the same magnetic field strength for every individual calculation of $q_I^{x,\mathrm{Berry}}$, $q_I^{y,\mathrm{Berry}}$, and $q_I^{z,\mathrm{Berry}}$, we may set $B_x = B_y = B_z = B$ and simplify the expression given in eq. (67). We further realize that the last contribution therein may be identified as the GAPT charge expression. This yields:

$$\langle q_I^{\mathrm{Berry}}\rangle_{\mathrm{rot}} = \frac{1}{6B}\sum_\alpha \varepsilon_{\alpha\beta\gamma}\frac{\partial p_\gamma}{\partial R_{I\beta}} + \frac{1}{2}q_I^{\mathrm{GAPT}}. \tag{68}$$

The expression given in eq. (68) demonstrates the relation between Berry and GAPT charges. Essentially, Berry charges are a mix of GAPT charges and another contribution which also resembles an atomic partial charge. The latter is obtained from the geometry gradient of the canonical momentum in the presence of a (vanishing) magnetic field. In the remainder of this work, we refer to this contribution as momentum partial charges and define them as:

$$q_I^{\mathrm{Mom}} = \frac{1}{3B}\sum_\alpha \varepsilon_{\alpha\beta\gamma}\frac{\partial p_\gamma}{\partial R_{I\beta}}\,. \tag{69}$$

Furthermore, we note that these momentum partial charges do not vanish in the absence of an external magnetic field. In the perturbative limit, they may be expressed as:

$$\lim_{|\mathbf{B}|\to 0} q_I^{\mathrm{Mom}} = \frac{1}{3}\varepsilon_{\alpha\beta\gamma}\left.\frac{\partial^2 p_\gamma}{\partial B_\alpha \partial R_{I\beta}}\right|_{|\mathbf{B}|=0}. \tag{70}$$

We close this section by pointing out that this division of the Berry charges in a GAPT and a momentum charge contribution is effectively a basis set artifact. As layed out in sec. II D,

the pseudomomentum-translational sum rule can be simplified in the limit of a complete basis. Following a similar derivation carried out in this section but starting from eq. (24) instead, we obtain:

$$\langle q_I^{\text{Berry}} \rangle_{\text{rot}} = q_I^{\text{GAPT}} \qquad \text{for basis} \to \infty. \tag{71}$$

In the limit of a complete basis and a vanishing magnetic field, Berry and GAPT charges are identical. It follows that the only difference we observe between the two variants of population analysis is a consequence of using an incomplete basis.

III. IMPLEMENTATION

A. Preface and notation

In this section, we describe our efficient integral-direct implementation of the Berry curvature into the TURBOMOLE[37–39] program suite. We largely follow the work presented by Culpitt, Peters, Tellgren, and Helgaker in Ref. 26. Therein, an analytical scheme for the calculation of the Berry curvature in the framework of generalized Hartree–Fock (GHF) was introduced. As such, we omit a detailed derivation here and instead highlight the specific features of our implementation that are novel.

We start by introducing some additional notation required for this section. We use ϕ_p for spinors, and subscripts i,j,k,l refer to occupied spinors while a,b refer to their virtual counterparts. All spinors are constructed in a linear combination of LAOs,[41,42] with Gaussian-type orbitals constituting the basis functions:

$$|p\rangle \coloneqq |\phi_p\rangle = \sum_\mu C_{\mu p} |\mu\rangle \,. \tag{72}$$

Here, $\mathbf{C}$ are the spinor coefficients. For the analytical calculation of the molecular Berry curvature, we need to consider derivatives with respect to nuclear displacements. We use the notation $|\phi_p^{I\alpha}\rangle$ to describe total derivatives with respect to a nuclear displacement and $|\phi_p^{(I\alpha)}\rangle$ for partial derivatives at fixed spinor coefficients. Perturbed spinor coefficients of the occupied–virtual block $U_{ai}^{I\alpha}$ are obtained from solving the coupled perturbed Hartree–Fock (CPHF) equations[61,69]

$$\begin{pmatrix} \mathbf{A} & \mathbf{B} \\ \mathbf{B}^* & \mathbf{A}^* \end{pmatrix} \begin{pmatrix} \mathbf{U}^{I\alpha} \\ \mathbf{U}^{I\alpha *} \end{pmatrix} = \begin{pmatrix} \mathbf{F}^{I\alpha} \\ \mathbf{F}^{I\alpha *} \end{pmatrix} , \tag{73}$$

where matrices $\mathbf{A}$ and $\mathbf{B}$ are given as

$$A_{ai,bj} = (\varepsilon_a - \varepsilon_i)\delta_{ij}\delta_{ab} + (ai||jb) \,, \tag{74}$$
$$B_{ai,bj} = (ai||bj) \,, \tag{75}$$

containing spinor energies ε_p and electron repulsion integrals given in the Mulliken notation. The efficient construction of perturbed Fock matrix $\mathbf{F}^{I\alpha}$ on the right-hand side (RHS) of eq. (73) will be the focus of sec. III C and details on solving the CPHF equations are given in sec. III D.

B. Construction of the molecular Berry curvature

For an electronic ground state, a convenient expression for the molecular Berry curvature can be derived in the framework of CPHF theory. Starting from the expression in eq. (5), we may obtain the following:[26]

$$\begin{aligned} \Omega_{I\alpha J\beta} = -2\,\mathrm{Im}\Bigg(& \sum_i \langle \phi_i^{(I\alpha)} | \phi_i^{(J\beta)} \rangle + \sum_{ia} U_{ai}^{I\alpha *} U_{ai}^{J\beta} \\ & + \sum_{ia} \langle \phi_a | \phi_i^{(J\beta)} \rangle U_{ai}^{I\alpha *} + \sum_{ia} \langle \phi_i^{(I\alpha)} | \phi_a \rangle U_{ai}^{J\beta} \\ & - \sum_{ij} \langle \phi_i^{(I\alpha)} | \phi_j \rangle \langle \phi_j | \phi_i^{(J\beta)} \rangle \Bigg) \,, \end{aligned} \tag{76}$$

which casts the molecular Berry curvature only in terms of perturbed molecular integrals with constant coefficients and the solutions of the CPHF equations $\mathbf{U}^{I\alpha}$. We note here that the first term in eq. (76) can be obtained in a straightforward fashion by contracting a perturbed two-center integral with the ground state total one electron density of the system:

$$\sum_i \langle \phi_i^{(I\alpha)} | \phi_i^{(J\beta)} \rangle = \sum_{\mu\nu} D_{0,\mu\nu} \langle \mu^{(I\alpha)} | \nu^{(I\alpha)} \rangle \,. \tag{77}$$

In GHF theory, the one-electron density

$$D_{\mu\nu} = \sum_i C_{\mu i} C_{\nu i}^* \tag{78}$$

may be decomposed into a total density and three spin densities according to

$$\mathbf{D} = \sum_{m=0}^{3} \mathbf{D}_m \otimes \boldsymbol{\sigma}_m \,, \tag{79}$$

with $\boldsymbol{\sigma}_m$ being the Pauli matrices and $m \in \{0,1,2,3\}$ representing the total (0) and spin (x,y,z) components, respectively. We further use the symbol $n \in \{1,2,3\}$ to refer only to the spin components in this work. For a more comprehensive introduction to GHF theory in the context of finite magnetic fields, the interested reader is referred to more specialized literature on that topic.[25,46,51]

We close this general discussion on the construction of the molecular Berry curvature by noting that $\langle \phi_a | \phi_i^{(I\alpha)} \rangle = \langle \phi_i^{(I\alpha)} | \phi_a \rangle^*$, which implies that only one of these integrals has to be computed. In our implementation, all $3N_{\text{nuc}}$ bra-sided derivative overlap integrals are constructed in the atomic orbital (AO) basis and subsequently transformed into the spinor basis. The occupied–occupied part of the resulting integrals are used for the fifth contribution in eq. (76), while the occupied–virtual part is used for the third and fourth contribution.

C. Construction of the perturbed Fock matrix

The only missing component is the perturbed spinor coefficient matrix $\mathbf{U}^{I\alpha}$. As previously mentioned, this is obtained

from solving the CPHF equations and obtaining it therefore constitutes the most time-consuming step in the calculation of the molecular Berry curvature. In our implementation, the computation of $\mathbf{U}$ consists of two parts. First, the construction of the perturbed Fock matrix, which is the RHS of eq. (73). Second, the iterative solution of the CPHF equations. Here, we start by focusing on the first part.

Following the derivations presented in Ref. 26, we obtain the following expression for the perturbed Fock matrix:

$$\mathrm{F}_{ai}^{I\alpha} = \varepsilon_i S_{ai}^{(I\alpha)} - F_{ai}^{(I\alpha)} + \sum_{kl} S_{kl}^{(I\alpha)} (ai||lk)\,. \tag{80}$$

For the first contribution, the perturbed overlap matrix $\mathbf{S}^{(I\alpha)}$ is calculated as the sum of a bra- and ket-derived overlap matrix in AO basis and subsequently transformed into the spinor basis. We only require the occupied–virtual part of this matrix here. In the second contribution, the derivative of the Fock matrix at constant spinor coefficients $F_{ai}^{(I\alpha)}$ requires us to calculate all integrals which are also necessary for the computation of geometry gradients. In the GHF framework, the contributions may be decomposed according to:[25,51]

$$\begin{aligned} F_{0,\mu\nu}^{(I\alpha)} &= h_{\mu\nu}^{(I\alpha)} + J_{\mu\nu}^{(I\alpha)} - K_{0,\mu\nu}^{(I\alpha)}\,, \\ F_{n,\mu\nu}^{(I\alpha)} &= -K_{n,\mu\nu}^{(I\alpha)} + {}^{\mathrm{Z}}F_{n,\mu\nu}^{(I\alpha)}\,. \end{aligned} \tag{81}$$

This contains the derivatives of the one-electron Hamiltonian $\mathbf{h}^{(I\alpha)}$, the Coulomb matrix $\mathbf{J}^{(I\alpha)}$, as well as the exchange matrix $\mathbf{K}^{(I\alpha)}$. Furthermore, the derivative of the spin Zeeman contribution ${}^{\mathrm{Z}}\mathbf{F}^{(I\alpha)}$ needs to be calculated. The Coulomb and exchange contributions contain derivatives of the four–center two-electron integrals which are contracted with the unperturbed density matrices

$$J_{\mu\nu}^{(I\alpha)} = \sum_{\kappa\lambda} \frac{\partial(\mu\nu|\kappa\lambda)}{\partial R_{I\alpha}} D_{0,\lambda\kappa}\,, \tag{82}$$

$$K_{m,\mu\nu}^{(I\alpha)} = \sum_{\kappa\lambda} \frac{\partial(\mu\lambda|\kappa\nu)}{\partial R_{I\alpha}} D_{m,\lambda\kappa}\,, \tag{83}$$

while the derivatives of the spin-Zeeman term are equivalent to derivatives of the overlap matrix scaled with the corresponding component of the magnetic field vector:

$${}^{\mathrm{Z}}F_{n,\mu\nu}^{(I\alpha)} = B_n S_{\mu\nu}^{(I\alpha)}\,. \tag{84}$$

The second contribution to the perturbed Fock matrix in eq. (80) may also be constructed in the AO basis and subsequently transformed into the spinor basis, where only the occupied–virtual block is required. It should be stressed again that all of these contributions are readily available in any quantum chemistry code that is already capable of computing a geometry gradient for molecules in a finite magnetic field.

We now turn to the third contribution in eq. (80), which contains the two-electron integrals in spinor basis, contracted with the derivative of the overlap matrix. At first glance, it appears as if a transformation of the four-center integrals into the spinor basis is unavoidable in the construction of the RHS of the CPHF equations. Such a transformation scales very unfavorably as $\mathcal{O}(N^5)$ with the system size. This expensive step would thus be a significant bottleneck in the calculation of the molecular Berry curvature. It can, however, be circumvented here. By transforming the entire third contribution in eq. (80) into the AO basis, we obtain after a few algebraic manipulations:[61,62]

$$\begin{aligned} \sum_{kl} S_{kl}^{(I\alpha)} (ai||lk) &= \sum_{kl}\sum_{\mu\nu} C_{\mu k}^* C_{\nu l} S_{\mu\nu}^{(I\alpha)} \sum_{\kappa\lambda} C_{\kappa l}^* C_{\lambda k} (ai||\kappa\lambda) \\ &= \sum_{\mu\nu\kappa\lambda} D_{\lambda\mu} D_{\nu\kappa} S_{\mu\nu}^{(I\alpha)} (ai||\kappa\lambda) \\ &= \sum_{\kappa\lambda} M_{\lambda\kappa}^{I\alpha} (ai||\kappa\lambda)\,. \end{aligned} \tag{85}$$

This expression may also be simplified to:

$$\sum_{kl} S_{kl}^{(I\alpha)} (ai||lk) = \sum_{\mu\nu} C_{\mu a}^* C_{\nu i} \sum_{\kappa\lambda} M_{\lambda\kappa}^{I\alpha} (\mu\nu||\kappa\lambda)\,. \tag{86}$$

Here, we have introduced the auxiliary matrix

$$\mathbf{M}^{I\alpha} = \mathbf{D}\mathbf{S}^{(I\alpha)}\mathbf{D}\,, \tag{87}$$

which is constructed in the AO basis. It has similar properties to a perturbed density matrix and is Hermitian. Any code capable of calculating the Coulomb and exchange matrices within the SCF procedure can therefore also be used to contract $\mathbf{M}^{I\alpha}$ with the four-center integrals instead. The result is transformed into the spinor basis and the occupied–virtual block of the result is equivalent to the third contribution in eq. (80). Through this scheme, the costly transformation of four-center integrals into the spinor basis is entirely avoided. The result is a fully integral-direct algorithm for the construction of the RHS of the CPHF equations. This had already been previously recognized for calculations of the geometry Hessian in the absence of external magnetic fields.[61,62]

D. Solving the CPHF equations

We conclude this section by briefly examining how the CPHF equations are solved in our implementation. The solver we use for this purpose is integral-direct and based on Davidson's method, which iteratively diagonalizes a subspace of the target matrix. This algorithm has been used in previous work for solving Casida's equation in the case of time-dependent Hartree–Fock. In the static case, Casida's equations and the CPHF equations are equivalent.[69]

The orbital rotation matrices $\mathbf{A}$ and $\mathbf{B}$ were defined in eqs. (74) and (75), respectively. Besides spinor energies, they consist of Coulomb and exchange integrals in the spinor basis. Similar to our procedure in sec. III C, we need to transform these two-electron integrals into the AO basis in order to obtain a formalism which can be implemented using an integral-direct algorithm. Having already constructed the RHS of CPHF in eq. (73), we can avoid having to fully construct the matrices $\mathbf{A}$ and $\mathbf{B}$ by realizing that only products with the solution vectors

$\mathbf{U}^{\chi}$ and $\mathbf{U}^{\chi*}$ are required. They are of the form

$$\mathrm{F}^{\chi}_{ai} = \sum_{jb} A_{ai,bj} \cdot U^{\chi}_{bj}, \tag{88}$$

$$= \sum_{jb} [(\varepsilon_a - \varepsilon_i)\delta_{ij}\delta_{ab} + (ai||jb)] \cdot U^{\chi}_{bj}, \tag{89}$$

with equivalent contributions from $\mathbf{B}$ and $\mathbf{U}^{\chi*}$. We use the more general perturbation parameter χ here instead of $I\alpha$ in order to differentiate the expressions given here from those on the RHS of the CPHF equations. The perturbed Fock matrix $\mathbf{F}^{\chi}$ is obtained as a linear combination of expressions such as those given in eq. (88). Evaluating the first term in eq. (89) is trivial and as such, we will focus on the second term. We transform this expression into the AO basis to obtain:

$$\sum_{jb}(ai||jb) \cdot U^{\chi}_{bj} = \sum_{\mu\nu} C^{*}_{\mu a} C_{\nu i} \sum_{jb} (\mu\nu||jb) \cdot U^{\chi}_{bj} \tag{90}$$

$$= \sum_{\mu\nu} C^{*}_{\mu a} C_{\nu i} \sum_{jb} \sum_{\kappa\lambda} C^{*}_{\kappa j} C_{\lambda b} (\mu\nu||\kappa\lambda) \cdot U^{\chi}_{bj} \tag{91}$$

$$= \sum_{\mu\nu} C^{*}_{\mu a} C_{\nu i} \sum_{\kappa\lambda} (\mu\nu||\kappa\lambda) \cdot \sum_{jb} C^{*}_{\kappa j} C_{\lambda b} U^{\chi}_{bj} \tag{92}$$

$$= \sum_{\mu\nu} C^{*}_{\mu a} C_{\nu i} \sum_{\kappa\lambda} (\mu\nu||\kappa\lambda) \cdot U^{\chi}_{\lambda\kappa}, \tag{93}$$

where we have defined the matrix elements as

$$U^{\chi}_{\lambda\kappa} = \sum_{jb} C_{\lambda b} U^{\chi}_{bj} C^{*}_{\kappa j}. \tag{94}$$

As such, the problem has been reduced to a contraction of the electron repulsion integrals with the perturbed coefficient matrices $\mathbf{U}^{\chi}$ in eq. (93), the solution of which has to be transformed into the spinor basis. As before, only the occupied–virtual block of the resulting matrix is required here. Please note that $\mathbf{U}^{\chi}$ is generally not Hermitian.

The procedure for obtaining the perturbed coefficient matrices $\mathbf{U}^{I\alpha}$ now works as follows: First, the RHS of the CPHF equations is constructed according to eq. (80) and stored on disk. Second, a starting guess for $\mathbf{U}^{I\alpha}$ is created and used to construct the left-hand side (LHS) according to the procedure described in this section, particularly eq. (93). Third, the LHS is compared to the RHS and from the difference, a new set of $\mathbf{U}$ vectors is created. This is done until the procedure is converged and the final set of solutions is written on disk for a subsequent calculation of different molecular quantities, including the molecular Berry curvature and the APT.

IV. COMPUTATIONAL METHODS

In the previous sections, we have derived the novel pseudomomentum-translational sum rule for the molecular Berry curvature. Furthermore, we have described our efficient, integral-direct algorithm capable of analytically computing the Berry curvature and other response properties for molecules in finite magnetic fields. We now use these tools to numerically validate the pseudomomentum-translational sum rule. Furthermore, we examine Berry charges of various molecules and compare them to the results obtained from other partial charge models. In particular, the connection between Berry and GAPT charges is investigated.

Unless stated otherwise, the molecular geometries presented in this work were optimized in the absence of an external magnetic field at the PBE/def2-TZVP level of theory.[70,71] Relatively large grids (grid 4) were employed for the numerical integration of the exchange-correlation functional.[72] The resolution of the identity approximation was used for the Coulomb part (RI-J) with an appropriate def2-TZVP auxilary basis set.[73] In the individual SCF cycles, the energies were converged up to at least $10^{-7}\,E_\mathrm{h}$. Geometries were optimized up to an energy of at least $10^{-6}\,E_\mathrm{h}$ and up to a gradient norm of at least $10^{-4}\,E_\mathrm{h}/a_0$.

For the numerical validation of the Berry curvature in sec. V A, we calculated the water molecule in an external magnetic field of magnitude $|\mathbf{B}| = 0.1\,B_0$ pointed in the direction $\mathbf{B} = (1,2,3)^{\top}$. This calculation was carried out on the GHF/def2-TZVP level of theory. Very tight convergence criteria were chosen: the energy was converged to $10^{-12}\,E_\mathrm{h}$ and the norm of the density matrix to 10^{-14}. The Berry curvature and all other response properties were obtained from a subsequent linear response calculations. Therein, the solution vectors were converged up to a norm of 10^{-10}.

The basis set convergence of Berry and GAPT charges is investigated in sec. V B. For this purpose, we have calculated the LiH molecule aligned in both a parallel and a perpendicular direction to the bond axis. The magnetic field strength was chosen to be $10^{-6}\,B_0 \approx 0.235\,\mathrm{T}$. All calculations were performed using GHF. Dunning basis sets of the type cc-pVXZ and aug-cc-pVXZ basis sets with X = D, T, Q, 5 were used for this investigation. SCF calculations were converged to $10^{-14}\,E_\mathrm{h}$ and the norm of the density matrix to 10^{-14}, while the solution vectors in the linear response calculations were converged up to a norm of 10^{-13}.

In sec. V C, results from different partial charge models are compared for the three heteroaromatic molecules furan, pyrrole, and thiophene. The geometries were optimized as previously described, but medium-sized grids (grid 3) were chosen for the numerical integration of the exchange-correlation functional. In sec. V D, trihalomethyl cations of the form CX_3^+ where X = F, Cl, Br are computed. Finally, the methylmagnesium bromide molecule was calculated. Here, we chose the PBE0 functional for the geometry optimization. Partial charges for all of these systems were obtained on the HF/def2-TZVP level of theory. Mulliken and Kollman charges were obtained from calculations in the absence of a magnetic field, while Berry and GAPT charges were obtained using the GHF method in an external magnetic field of $10^{-4}\,B_0 \approx 23.5\,\mathrm{T}$. The SCF calculations were converged to $10^{-12}\,E_\mathrm{h}$ in the energy and 10^{-14} in the norm of the density matrix. Linear response solution vectors were converged up to a norm of 10^{-10}.

V. RESULTS AND DISCUSSION

A. Numerical validation of the novel sum rule

The novel pseudomomentum-translational sum rule was presented and derived in secs. II C – II E of this work. We start this discussion by validating it numerically for one example, relating it also to the APT and the geometry gradient of the canonical momentum operator. As a test case, we chose the water molecule in an external magnetic field of $|\mathbf{B}| = 0.1\,B_0$ pointed in the direction $\mathbf{B} = (1,2,3)^\top$. This is equivalent to a magnetic field of $\mathbf{B} \approx (0.0267261, 0.0534522, 0.0801784)^\top$. The water molecule was chosen to lie in the xz-plane and consequently, the overall system has C_1 symmetry.[74]
We have calculated the molecular Berry curvature of this system, alongside the geometry gradients of the canonical momentum and the electronic dipole moment. The values are depicted in fig. 1. Therein, we have also evaluated the pseudomomentum-translational sum rule according to eq. (6) as indicated in red and the magnetic-translational sum rule[27] according to eq. (8), which is highlighted in blue here. Furthermore, the geometry gradient of the electronic pseudomomentum was evaluated according to eq. (17), which is also indicated in red within the figure.
Evidently, the pseudomomentum-translational sum rule leads to a matrix with identical values to those found in the geometry gradient of the electronic pseudomomentum. While only 7 digits are depicted here, they agree up to the precision of the reference calculation, which in this case is at least 10 digits. By summing over an additional atomic index, the magnetic-translational sum rule is obtained. For the water molecule with $N_{\mathrm{el}} = 10$, it can be clearly seen that it matches up with the magnetic field tensor shown in eq. (9). All of these findings clearly demonstrate the validity of both translational sum rules for the molecular Berry curvature. While this system is only one example, we demonstrate this also for all other systems investigated in the context of this work. The supporting information lists both the molecular Berry curvature as well as the geometry gradients of the electric dipole moment, canonical momentum, and the electronic pseudomomentum.

B. Basis set convergence of Berry and GAPT charges

In sec. II F, we have reintroduced the concept of isotropic Berry charges originally proposed in Ref. 24. Their close relation to GAPT charges[35,36] was explicitly shown in sec. II G of this work using the pseudomomentum-translational sum rule. Having validated the sum rule numerically, we now turn our focus on comparing Berry charges to GAPT charges. Of particular interest in this investigation is the consideration of the basis set limit given in eq. (71), which was derived using the pseudomomentum-translational sum rule. To reiterate, Berry and GAPT charges become equivalent in the limit of a complete basis. In this section, we demonstrate that individual APT charges may also be related to elements of the atomic pseudomomentum tensor in eq. (50). For a magnetic field aligned with the Cartesian z-component, $\mathbf{B} = (0,0,B_z)^\top$, this relation was explicitly shown in eqs. (64) – (65). Furthermore, we introduce individual momentum partial charges corresponding to the elements of the atomic pseudomomentum tensor:

$$q_I^{xy,\mathrm{Mom}} = \frac{2}{B_z}\frac{\partial p_y}{\partial R_{Ix}}\,, \tag{95}$$

$$q_I^{yx,\mathrm{Mom}} = -\frac{2}{B_z}\frac{\partial p_x}{\partial R_{Iy}}\,. \tag{96}$$

A similar set of partial charges can be defined for other directions of the magnetic field vector. The isotropic average of their linear combination was shown in eq. (69). In a complete basis, the relation between APT charges, momentum charges, and the atomic pseudomomentum tensor elements becomes:

$$q_I^{x,\mathrm{APT}} = q_I^{xy,\mathrm{Mom}} = \omega_{I,xy}/B_z\,, \tag{97}$$

$$q_I^{y,\mathrm{APT}} = q_I^{yx,\mathrm{Mom}} = -\omega_{I,yx}/B_z\,. \tag{98}$$

As a model system, we chose the lithium hydride molecule in a very small magnetic field of $B_z = 10^{-6}B_0$ applied in parallel direction to the bond axis. To assess the basis set limit, we evaluated the molecular Berry curvature and the APT charges using the basis sets (aug-)cc-pVXZ (X = D, T, Q, 5). Due to the C_∞ symmetry of the system,[74] the atomic pseudomomentum tensor $\boldsymbol{\omega}_I$ becomes antisymmetric: $\omega_{I,xy} = -\omega_{I,yx}$. For the same reason, the two relevant APT charges become equivalent in this case: $q^{x,\mathrm{APT}} = q^{y,\mathrm{APT}}$. As such, we only have to compare the APT charge $q^{y,\mathrm{APT}}$ to the atomic pseudomomentum tensor element $\omega_{I,yx}$. The same is true for the respective momentum charges. The results are presented in table I for the hydrogen atom in LiH.

Basis set	$q_{\mathrm{H}}^{y,\mathrm{APT}}$	$q_I^{yx,\mathrm{Mom}}$	$-\omega_{\mathrm{H},yx}/B_z$
cc-pVDZ	–1.7725	–1.6628	–1.7176
cc-pVTZ	–1.7777	–1.7533	–1.7655
cc-pVQZ	–1.7801	–1.7718	–1.7760
cc-pV5Z	–1.7810	–1.7783	–1.7797
aug-cc-pVDZ	–1.7844	–1.7809	–1.7827
aug-cc-pVTZ	–1.7818	–1.7770	–1.7794
aug-cc-pVQZ	–1.7815	–1.7803	–1.7809
aug-cc-pV5Z	–1.7815	–1.7810	–1.7812

TABLE I. Comparison between one APT charge, one momentum charge and the corresponding element of the atomic pseudomomentum tensor divided by the magnetic field strength. A magnetic field of $10^{-6}\,B_0$ was applied in parallel direction to the bond axis of LiH. The calculations were performed using Hartree–Fock. Different Dunning basis sets are considered to assess the basis set convergence. All values are given in units of $[e]$.

The basis set convergence is clearly visible for the APT charge $q_{\mathrm{H}}^{y,\mathrm{APT}}$, the momentum charge $q_I^{yx,\mathrm{Mom}}$, and the atomic pseudomomentum tensor element $\omega_{\mathrm{H},yx}/B_z$. The APT charge converges faster against the basis set limit compared to the other two, but all of them eventually converge against the same limit. Please note that the atomic pseudomomentum tensor element is the average of the APT and momentum charge. In the largest basis considered here, aug-cc-pV5Z, the difference

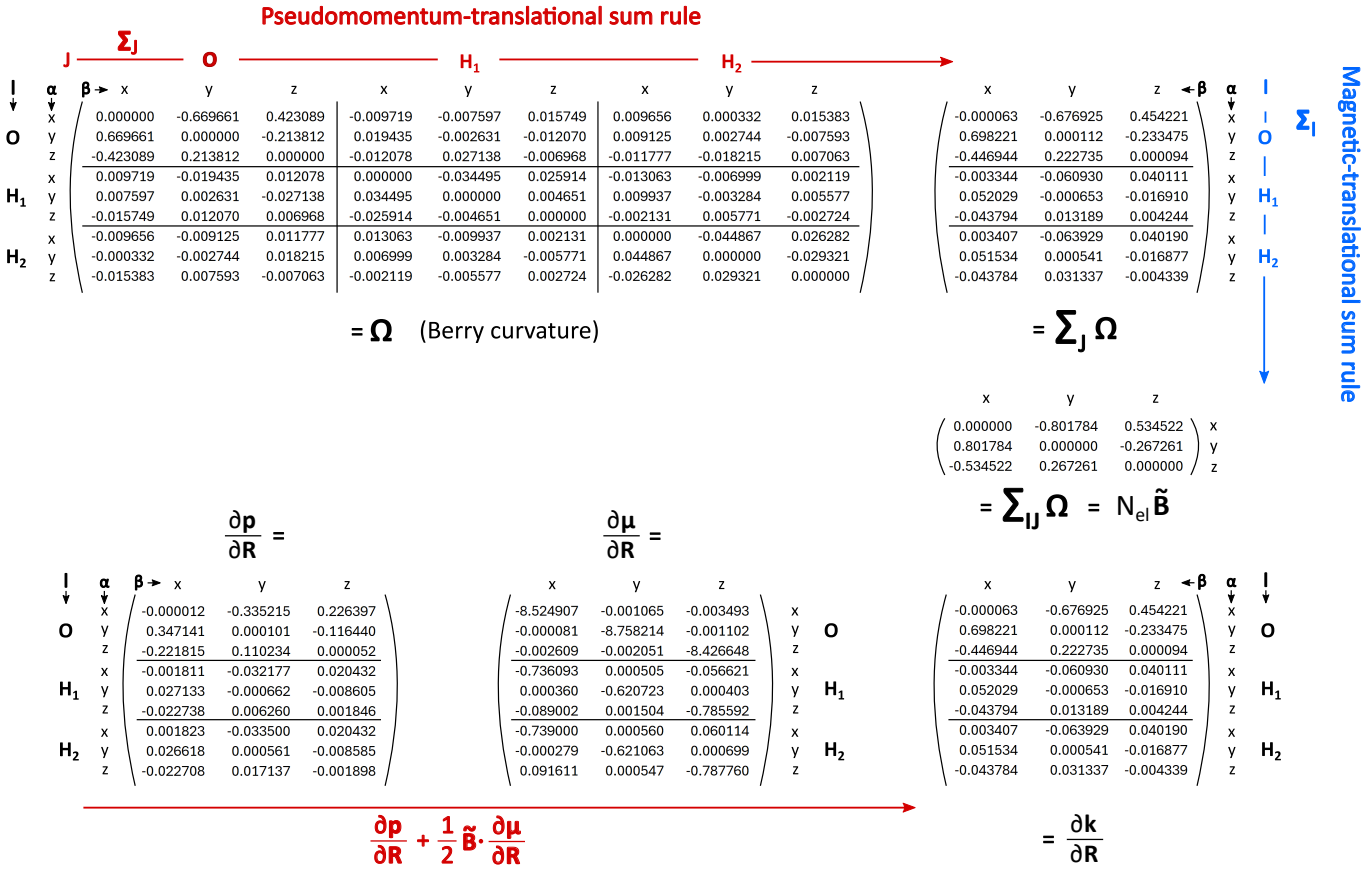

FIG. 1. Schematic depiction of how to evaluate the translational sum rules of the molecular Berry curvature for the water molecule in a skewed external magnetic field. The molecular Berry curvature is shown with labels indicating its components. Summing over one atomic index is equivalent to evaluating the pseudomomentum-translational sum rule, indicated here in red. Subsequently summing over the other atomic index is equivalent to evaluating the magnetic-translational sum rule,[27] indicated here in blue. As a comparison, the geometry gradients of the canonical momentum and electronic dipole moment are shown. From these, the geometry gradient of the electronic pseudomomentum was calculated. This matches perfectly with the results obtained from the pseudomomentum-translational sum rule.

between the APT and momentum charge is only $0.0005\,e$, which is about 0.03%. It is unsurprising that the momentum charge and therefore also the atomic pseudomomentum tensor element converges more slowly against the basis set limit compared to the APT charge. The basis set requirements for the pseudomomentum were already discussed in sec. II D – it is a composite quantity, constructed from both the electric dipole moment and the canonical momentum. While the former has an exact representation in coordinate space, the latter only has one in momentum space. As such, the basis we provide (which is in real space) leads to a rapid convergence of the APT charge. In comparison, the pseudomomentum needs a larger basis in real space to converge.

Next, we consider the LiH molecule in a magnetic field applied in perpendicular direction to the bond axis. Due to the symmetry reduction to C_s,[74] the atomic pseudomomentum tensor is no longer antisymmetric and the APT charges are no longer equivalent: $q^{x,\mathrm{APT}} \neq q^{y,\mathrm{APT}}$. Thus, we need to consider them separately. The results for the hydrogen atom in LiH are presented in table II. First, we note that the results for the APT charge $q_{\mathrm{H}}^{y,\mathrm{APT}}$, the momentum charge $q_I^{yx,\mathrm{Mom}}$, and the corresponding atomic pseudomomentum tensor element $\omega_{\mathrm{H},yx}/B_z$ are exactly the same as for LiH in a parallel field. However, for the other set of charges, we can observe a slower convergence to the basis set limit compared to the parallel case.

Basis set	$q_{\mathrm{H}}^{x,\mathrm{APT}}$	$q_I^{xy,\mathrm{Mom}}$	$\omega_{\mathrm{H},xy}/B_z$	$q_{\mathrm{H}}^{y,\mathrm{APT}}$	$q_I^{yx,\mathrm{Mom}}$	$-\omega_{\mathrm{H},yx}/B_z$
cc-pVDZ	–1.4326	–1.3151	–1.3738	–1.7725	–1.6628	–1.7176
cc-pVTZ	–1.4780	–1.4554	–1.4667	–1.7777	–1.7533	–1.7655
cc-pVQZ	–1.4818	–1.4635	–1.4727	–1.7801	–1.7718	–1.7760
cc-pV5Z	–1.4860	–1.4753	–1.4806	–1.7810	–1.7783	–1.7797
aug-cc-pVDZ	–1.4639	–1.4392	–1.4515	–1.7844	–1.7809	–1.7827
aug-cc-pVTZ	–1.4882	–1.4361	–1.4622	–1.7818	–1.7770	–1.7794
aug-cc-pVQZ	–1.4883	–1.4884	–1.4884	–1.7815	–1.7803	–1.7809
aug-cc-pV5Z	–1.4882	–1.4885	–1.4883	–1.7815	–1.7810	–1.7812

TABLE II. Comparison between the two non-redundant APT charges, momentum charges and the corresponding elements of the atomic pseudomomentum tensor divided by the magnetic field strength. A magnetic field of $10^{-6}\,B_0$ was applied in perpendicular direction to the bond axis of LiH. The calculations were performed using Hartree–Fock. Different Dunning basis sets are considered to assess the basis set convergence. All values are given in units of $[e]$.

Particularly the non-augmented basis sets of type cc-pVXZ converge very slowly, with a difference of $0.01\,e$ between the APT and momentum charge in the case of cc-pV5Z, which amounts to about 0.7%. It should be noted that the augmented basis sets perform significantly better. The aug-cc-pVQZ basis set appears to be sufficient for a convergence of both the APT and momentum charges, yielding results that agree up to the numerical accuracy of the reference calculation.
These findings confirm the expected basis set convergence of the APT and momentum charges, and thereby also the Berry charges. However, we want to point out a peculiar convergence pattern visible for the momentum charge in table II. While the APT charges are already converged for the aug-cc-pVTZ basis set, the momentum charge $q_I^{yx,\mathrm{Mom}}$ is still off by more than $0.05\,e$, which corresponds to an error of about 3.5%. Curiously, the non-augmented cc-pVTZ basis yields a value which is closer to the aug-cc-pV5Z reference, differing only by approximately 2.2%. Why does the augmented basis yield a worse result for the 3ζ basis compared to its non-augmented counterpart? To analyze this, we have performed further calculations for LiH in a perpendicular magnetic field with the aug-cc-pVTZ basis set in which we have subsequently discarded some of the additional diffuse functions. The results are listed in table III.

Basis set	$q_{\mathrm{H}}^{x,\mathrm{APT}}$	$q_{\mathrm{H}}^{xy,\mathrm{Mom}}$	$q_{\mathrm{H}}^{y,\mathrm{APT}}$	$q_{\mathrm{H}}^{yx,\mathrm{Mom}}$
H w/o aug(s)	–1.4869	–1.4178	–1.7816	–1.7773
H w/o aug(p)	–1.4890	–1.5131	–1.7823	–1.7802
H w/o aug(d)	–1.4892	–1.5048	–1.7818	–1.7700
H w/o aug(p,d)	–1.4897	–1.5135	–1.7815	–1.7729
H w/o aug(s,p,d)	–1.4871	–1.5002	–1.7813	–1.7706
Li w/o aug(s)	–1.4880	–1.4325	–1.7817	–1.7765
Li w/o aug(p)	–1.4881	–1.4321	–1.7818	–1.7781
Li w/o aug(d)	–1.4878	–1.4340	–1.7816	–1.7787
Li w/o aug(f)	–1.4883	–1.4479	–1.7817	–1.7773

TABLE III. APT and momentum charges for LiH with a magnetic field of $10^{-6}\,B_0$ applied in perpendicular direction to the bond axis. The calculations were performed using Hartree–Fock. All calculations were performed with a modified aug-cc-pVTZ basis, in which some of the additional diffuse functions were discarded as indicated. All values are given in units of $[e]$.

The APT charges are almost not affected by the change in the basis set, with the largest differences being of approximately $0.002\,e$. The momentum charges, on the other hand, are heavily affected by the presence of the diffuse functions in the aug-cc-pVTZ basis. This is particularly true for the additional diffuse functions on the hydrogen atom for the $q_{\mathrm{H}}^{xy,\mathrm{Mom}}$ charge. Differences here are almost $0.1\,e$, which is two orders of magnitude larger than differences visible for the APT charges. The presence of the diffuse p- and d-functions in the augmented basis set appears to be particularly important for the momentum charge. Discarding these functions leads to a significantly more negatively charged hydrogen atom compared to the result obtained from the aug-cc-pVTZ basis. It should be noted that the $q_{\mathrm{H}}^{xy,\mathrm{Mom}}$ charges become even more negative than the one obtained from the aug-cc-pV5Z basis.
As previously discussed in sec. II D, we expected the momentum and therefore also the momentum charges to converge significantly slower to the basis set limit than the electric dipole moment and the APT charges. The diffuse functions are essential here because the external magnetic field induces a plane-wave character into the electronic wave function, which needs to be captured by the basis in coordinate space. This implies that the molecular Berry curvature might also be affected by such basis set convergence issues. Depending on the molecular system, some coordinates of the molecular Berry curvature may converge significantly faster than others with the basis set size. Future investigations for molecules in finite magnetic fields should take this effect into account when choosing a basis.

C. Dipole moments of heteroaromatic molecules

Having examined the basis set convergence of Berry and GAPT charges, we now compare their general performance to Mulliken charges[28–30] as well as partial charges obtained from an electrostatic potential fit based on Kollman's parametrization.[34] Since partial charges are not observable quantities, we cannot directly compare them to reference data. However, properties constructed from them – such as the electric dipole moment – can be used to assess the quality of a population analysis. In this section, we therefore investigate the electric dipole moment of various molecules, comparing the results obtained from the aforementioned types of population analyses to the quantum-mechanical definition given in eq. (19).
As model systems, we chose the five-membered heteroaromatic molecules furan, pyrrole, and thiophene. All of them are planar and their structures are shown in fig. 2. These molecules are particularly interesting for this investigation because pyrrole is known to have an inverse electric dipole moment compared to furan and thiophene.[75] We expect the different types of population analysis to predict this feature at least qualitatively correct.

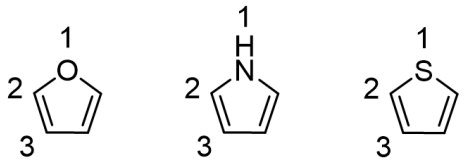

FIG. 2. Molecular structures of furan, pyrrole and thiophene with numbers indicating different positions.

The classical definition of an electric dipole moment is a sum over charges and their respective coordinates. For partial charges, we can make the assumption that they are located exactly at the nuclear position of their respective atoms:

$$\mu_\alpha \overset{!}{=} \sum_I q_I(\mathbf{R}) \cdot R_{I\alpha}\,. \tag{99}$$

However, this construction can lead to a conceptual problem. The derivative of the dipole moment with respect to an atomic coordinate yields[36]

$$\frac{\partial \mu_\alpha}{\partial R_{J\beta}} = q_J(\mathbf{R})\,\delta_{\alpha\beta} + \sum_I \frac{\partial q_I(\mathbf{R})}{\partial R_{J\beta}} \cdot R_{I\alpha}\,, \tag{100}$$

which does not satisfy the classical relation between charges and dipole moments. The problem is the dependence of the partial charge's magnitude on its position in space – classical charges do not exhibit any such dependency. Instead of assuming that the partial charges add up to the electric dipole moment, we could also require them to yield the correct relation to the derivative of the dipole moment:

$$\frac{\partial \mu_\alpha}{\partial R_{J\beta}} \stackrel{!}{=} q_J(\mathbf{R})\delta_{\alpha\beta}\,. \tag{101}$$

However, with this choice we lose information about the connection between partial charges and the electric dipole moment. Trying to solve eq. (101) for $\boldsymbol{\mu}$, we quickly realize that we would have to arbitrarily define an integration constant.

As such, partial charges can – except for a few special cases – only fulfill either eq. (99) *or* eq. (101). It should be noted that usually, partial charges derived from any type of population analysis will fulfill neither of these two equations perfectly. However, their construction might already suggest that they will yield more reasonable results for either one of these conditions. For APT charges (and the closely related Berry charges), the second condition is already fundamental to their construction. Hence, we do not necessarily expect them to yield reasonable results for the electric dipole moment if it is calculated according to eq. (99). Kollman charges, on the other hand, are obtained from an electrostatic potential fit. As such, they are much more closely aligned to the first condition and should yield reasonable results for the electric dipole moment. Mulliken charges are constructed directly from the density matrix and are therefore not necessarily linked to either of those conditions.

As pointed out in Ref. 76, planar molecules present a special case. For a molecule in the xz-plane, the derivatives $\partial q_I/\partial R_{Jy}$ will vanish due to symmetry reasons. Therefore, the APT charge $\mathrm{APT}^{yy} = q_I^{\mathrm{y}}$ corresponds exactly to the electric dipole moment here. A similar relation can be derived for the Berry charges. Following from the connection to the APT charges, the linear combination

$$q_I^{x+z-y,\mathrm{Berry}} = q_I^{x,\mathrm{Berry}} + q_I^{z,\mathrm{Berry}} - q_I^{y,\mathrm{Berry}} \tag{102}$$

$$= 3\,\langle q_I^{\mathrm{Berry}}\rangle_{\mathrm{rot}} - 2q_I^{y,\mathrm{Berry}} \tag{103}$$

corresponds to the APT charge q_I^{y}. They are equivalent in the limit of a complete basis. In the remainder of this section, we will take these two special cases (APT^{yy} and Berry^{x+z-y}) into account.

We start this discussion with the furan molecule. The partial charges for all nonequivalent atoms are presented in table IV. As expected, Berry and GAPT charges are very similar to one another, with the biggest difference of less than $0.02\,e$ being the partial charge predicted for the oxygen atom. The

Atom	Berry	Berry^{x+z-y}	GAPT	APT^{yy}	Mulliken	Kollman
1O	–0.4978	–0.1540	–0.5159	–0.1702	–0.3373	–0.1206
2C	0.1582	–0.0896	0.1669	–0.0817	0.0581	–0.1127
3C	–0.0719	–0.2111	–0.0792	–0.2157	–0.1839	–0.1916
2H	0.0909	0.1982	0.0926	0.2000	0.1530	0.1906
3H	0.0716	0.1794	0.0776	0.1824	- 0.1414	0.1741

TABLE IV. Partial charges calculated for furan on the HF/def2-TZVP level of theory. The numbering of the atoms follows from figure 2, hydrogen atoms are tagged with the number of the respective atom they are bound to. All values in $[e]$.

APT^{yy} and Berry^{x+z-y} charges agree similarly well with one another, but show extreme discrepancies to the APT and Berry charges, respectively. For oxygen, this difference is approximately $0.35\,e$, and we even find a qualitative difference for the 2C atom, with Berry and GAPT charges predicting positive partial charges, while the APT^{yy} and Berry^{x+z-y} charges are negative. Mulliken charges qualitatively agree with Berry and GAPT charges. Kollman charges, on the other hand, agree with APT^{yy} and Berry^{x+z-y} charges. The biggest difference is only about $0.05\,e$ and can be found for the oxygen atom when comparing the APT^{yy} and Kollman charge.

For pyrrole, partial charges obtained from the different population analyses are listed in table V. As expected, Berry and APT charges are in good agreement, with the biggest difference of about $0.04\,e$ for the nitrogen atom. APT^{yy} and Berry^{x+z-y} charges again show large differences to APT and Berry charges, predicting much more electronegative carbon atoms and a much more electropositive nitrogen atom. The differences between these two types of partial charges is somewhat larger, with the biggest difference of about $0.06\,e$ being found on the nitrogen atom. Mulliken charges are in relatively good agreement with the APT^{yy} charges compared to furan. Kollman charges, on the other hand, show a much bigger discrepancy here, with differences of almost $0.2\,e$ for the nitrogen atom compared to the respective APT^{yy} charge. Kollman charges predict significantly more electronegative carbon atoms for pyrrole compared to the other methods.

Atom	Berry	Berry^{x+z-y}	GAPT	APT^{yy}	Mulliken	Kollman
1N	–0.3512	–0.2285	–0.3895	–0.2910	–0.3214	–0.1083
1H	0.2379	0.3094	0.2511	0.3239	0.2511	0.3030
2C	0.0206	–0.1883	0.0371	–0.1423	–0.0608	–0.2847
3C	–0.0949	–0.2321	–0.1094	–0.2654	–0.1771	–0.1946
2H	0.0766	0.2051	0.0778	0.2016	0.1451	0.2088
3H	0.0543	0.1748	0.0638	0.1896	0.1280	0.1732

TABLE V. Partial charges calculated for pyrrole on the HF/def2-TZVP level of theory. The numbering of the atoms follows from figure 2, hydrogen atoms are tagged with the number of the respective atom they are bound to. All values in $[e]$.

The partial charges for thiophene are listed in table VI. Here, Berry and GAPT charges are even closer to one another than for the other two molecules. They both predict a slightly negative charge on the sulfur atom, whereas all other models predict a positive charge. The largest difference between Berry^{x+z-y} and APT^{yy} charges can be found for the 2C atom,

approximately 0.01 e. Kollman charges are relatively close to the two aforementioned types of population analyses, with the largest difference of about 0.04 e for the sulfur atom. Mulliken charges are in a qualitative agreement to Kollman, APT^{yy}, and Berry^{x+z-y} charges, but overestimate the electropositive character of sulfur, while underestimating the electronegative character of the 2C atom.

Atom	Berry	Berry^{x+z-y}	GAPT	APT^{yy}	Mulliken	Kollman
1S	–0.0515	0.0973	–0.0647	0.0897	0.1427	0.0539
2C	–0.0129	–0.2704	–0.0007	–0.2484	–0.1893	–0.2785
3C	–0.0920	–0.1409	–0.1082	–0.1666	–0.1734	–0.1357
2H	0.0780	0.1895	0.0818	0.1885	0.1568	0.2294
3H	0.0527	0.1731	0.0595	0.1816	0.1346	0.1579

TABLE VI. Partial charges calculated for thiophene on the HF/def2-TZVP level of theory. The numbering of the atoms follows from figure 2, hydrogen atoms are tagged with the number of the respective atom they are bound to. All values in $[e]$.

The electric dipole moments for all three molecules as calculated from the different types of population analyses are presented in table VII. In addition, the electric dipole moment evaluated according to eq. (19) from the density of the HF calculation is given here. This value is taken as the reference, and the difference between the dipole moments evaluated via the partial charge models and this reference is visualized in fig. 3.

Model	Furan	Pyrrole	Thiophene
Density	–0.3123	0.7573	–0.2760
Berry	–0.8278	0.4373	–0.0191
Berry^{x+z-y}	–0.2888	0.7637	–0.3110
GAPT	–0.8655	0.4208	–0.0225
APT^{yy}	–0.3123	0.7573	–0.2760
Mulliken	–0.4808	0.4397	0.2265
Kollman	–0.3046	0.7535	–0.2641

TABLE VII. Electric dipole moments for furan, pyrrole, and thiophene. 'Density' refers to the expectation value of the dipole moment operator calculated from the ground state density. The other dipole moments were evaluated using their respective partial charge models. All values in $[ea_0]$.

First, we notice that almost all partial charge models predict the correct sign for the electric dipole moments of the heteroaromatic molecules, with pyrrole showing the aforementioned characteristic inverse dipole moment. However, from a quantitative point of view, the results differ drastically. For furan, the results obtained from Berry and GAPT charges differ from the reference by more than 0.5 ea_0, yielding an electric dipole moment which is almost three times larger than the reference value. For thiophene, Berry and GAPT charges predict an almost vanishing electric dipole moment, while the reference has a value of $-0.2760\,ea_0$. Generally, Berry and GAPT charges do not appear to be suitable for accurately predicting the electric dipole moment. While this had been noted for GAPT charges in the literature,[36] we also want to highlight this deficiency for Berry charges here.
Mulliken charges also perform poorly in the description of the

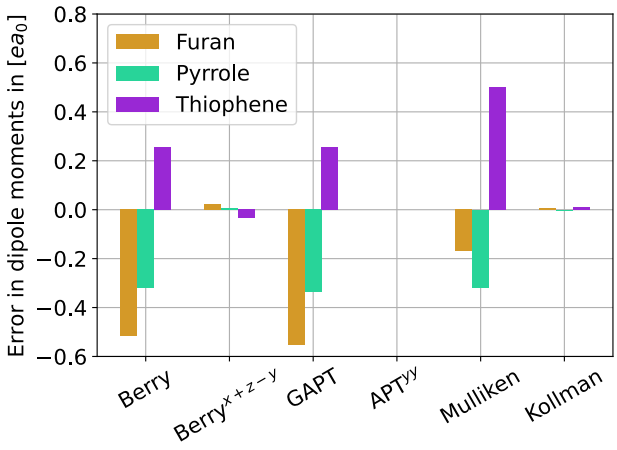

FIG. 3. Difference between electric dipole moments calculated from different partial charge models and the reference value which was calculated from the density. See also table VII.

electric dipole moments. For the thiophene molecule in particular, they predict the wrong direction of the electric dipole moment, thereby failing even in a qualitatively correct description of this property. While they predict the correct sign for furan and pyrrole, differences of more than 0.3 ea_0 to the reference value can be observed.
As previously discussed, APT^{yy} charges are expected to yield exactly the same results as the reference.[36,76] This is observed here as well, with the two matching up to the accuracy of the calculation, which in this case is at least 10 digits. As expected, Berry^{x+z-y} charges yield very similar results with differences of up to about 0.03 ea_0 compared to the reference. As previously discussed, the discrepancy between APT^{yy} and Berry^{x+z-y} charges should mostly be seen as a basis set artifact. Kollman charges yield very similar values to the reference as well, with errors of only about 0.01 ea_0.
The good performance of APT^{yy}, Berry^{x+z-y}, and Kollman charges is clearly visible in fig. 3. However, it should be stressed again that the heteroaromatic systems investigated here are a special case. For non-planar molecules, there are generally no linear combinations of Cartesian components of either the APT or Berry charges that lead to such a good agreement with an appropriate reference.[77] GAPT charges and the closely related Berry charges generally describe molecular properties such as the electric dipole moment poorly. They can, however, be very useful to model charge fluctuation during molecular motion.[36] For GAPT charges, this is relevant in the case of infrared spectroscopy, while Berry charges can be useful for the description of molecular rotations and vibrations in strong magnetic fields.[20,27]

D. Partial charges of molecules with strong ionic character

In this section, we compare the performance of the different partial charge models for molecules with strong

ionic character. Relatively high charges are expected for some of the atoms contained in these molecules, and they present a challenge for any type of population analysis. Our first model systems are trihalomethyl cations,[78,79] which are molecules of the form CX_3^+ where X = F, Cl, Br. The resonance structure of this system is depicted in fig. 4. For the investigation of partial charges, these molecules are particularly interesting because the carbon atom is known to become increasingly electronegative in the homologous series from CF_3^+ to CBr_3^+.[80,81] We expect this trend to be reflected in the partial charges of the system.

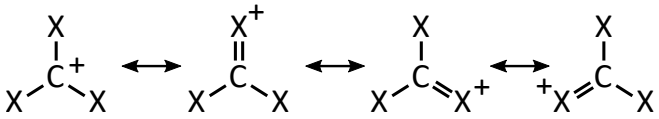

FIG. 4. Resonance structures of the trihalomethyl cation CX_3^+ with X = F, Cl, Br.

The partial charges evaluated from the four aforementioned types of population analysis (Berry, GAPT, Mulliken, and Kollman charges) are presented in table VIII. Due to the symmetry of the molecular system, there is no distinction between partial charges of different halogen atoms within the individual structures. The partial charge at the carbon atom is indicated as $\mathbf{C}X_3^+$, while the partial charge at the halogen atom is indicated as $C\mathbf{X}_3^+$.

Atom	Berry	GAPT	Mulliken	Kollman
$\mathbf{C}F_3^+$	2.0009	2.0457	0.9768	0.9976
$\mathbf{C}Cl_3^+$	1.4241	1.4497	0.1761	–0.1304
$\mathbf{C}Br_3^+$	1.1845	1.2038	0.0527	–0.3179
$C\mathbf{F}_3^+$	–0.3336	–0.3486	0.0077	0.0008
$C\mathbf{Cl}_3^+$	–0.1414	–0.1499	0.2746	0.3768
$C\mathbf{Br}_3^+$	–0.0615	–0.0679	0.3158	0.4397

TABLE VIII. Partial charges in $[e]$ for CX_3^+ with X = F, Cl, Br. All calculations were performed on the HF/def2-TZVP level of theory. Berry and GAPT charges were evaluated at $|\mathbf{B}| = 10^{-4}B_0$.

The data is further visualized in fig. 5. Overall, the trend of an increasingly electronegative carbon atom is reproduced by all types of population analysis. Berry and GAPT charges are relatively close to one another in all cases, with the largest difference being less than $0.05\,e$ (2.2%) for the carbon atom in CF_3^+. Differences to Mulliken and Kollman charges are much more pronounced, more than $1\,e$ in all instances. While the Berry and GAPT population analyses predict a charge of about $+2e$ for the carbon atom of CF_3^+, Mulliken and Kollman only predict one of about $+1\,e$. For CCl_3^+ and CBr_3^+, the differences become even more drastic. The Kollman population analysis predicts negative partial charges on carbon, while Berry and GAPT charges both predict a heavily ionic ($> +1e$) carbenium ion. The presence of a heavily cationic carbenium ion for these molecules is not supported by experimental data, the interested reader is referred to Ref. 81 for a detailed report on this issue. Therefore, this large discrepancy between Kollman and GAPT/Berry charges should be interpreted as a deficiency of the latter two.

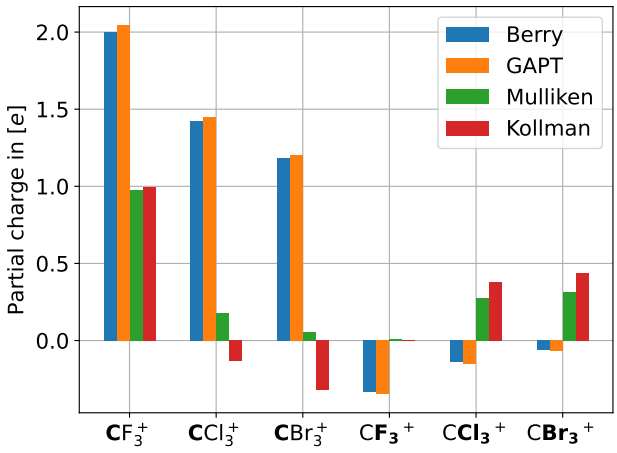

FIG. 5. Visualization of the partial charges in $[e]$ for CX_3^+ with X = F, Cl, Br presented in table VIII.

We now turn our attention to another species: methylmagnesium bromide. Partial charges obtained from the different models are listed in table IX and visualized in fig. 6. In contrast to the CX_3^+, all partial charge models appear to at least qualitatively agree with one another. As expected, Berry and GAPT charges are very similar in all cases, while there are some larger differences compared to Mulliken and Kollman charges. For the magnesium atom, both GAPT and Berry charges predict a partial charge of about $+1.15\,e$, while Kollman predicts a partial charge of only about $+0.81\,e$. This is a difference of more than 40% if the Kollman charge is taken as the reference value. For the carbon atom, differences of approximately $0.2\,e$ are obtained. This corresponds to similarly large relative error compared to the Kollman charge. For the bromine atom, we also get differences of approximately $0.2\,e$, corresponding to an error of about 40%.

Atom	Berry	GAPT	Mulliken	Kollman
C	–0.3141	–0.3461	–0.7914	–0.5308
H	–0.0504	–0.0430	0.1319	0.0638
Mg	1.1341	1.1579	0.9158	0.8076
Br	–0.6689	–0.6827	–0.5202	–0.4682

TABLE IX. Partial charges in $[e]$ for CH_3MgBr. All calculations were performed on the HF/def2-TZVP level of theory. Berry and GAPT charges were evaluated at $|\mathbf{B}| = 10^{-4}B_0$.

To summarize, Berry and GAPT charges yield very similar results for the molecules investigated here. This is to be expected due to their close connection via the pseudomomentum-translational sum rule. In a complete basis, Berry and GAPT charges would be equivalent, but even in finite basis sets commonly used in quantum chemical calculations, the two models predict very similar partial charges. Berry charges therefore suffer from the same deficiencies as GAPT charges.[36,77] Compared to other models such as partial charges obtained from an electrostatic potential fit based

on Kollman's parametrization, Berry and GAPT charges predict quantitatively and in some instances even qualitatively different results. This problem is especially egregious for the more challenging molecules with strong ionic character considered in this section.

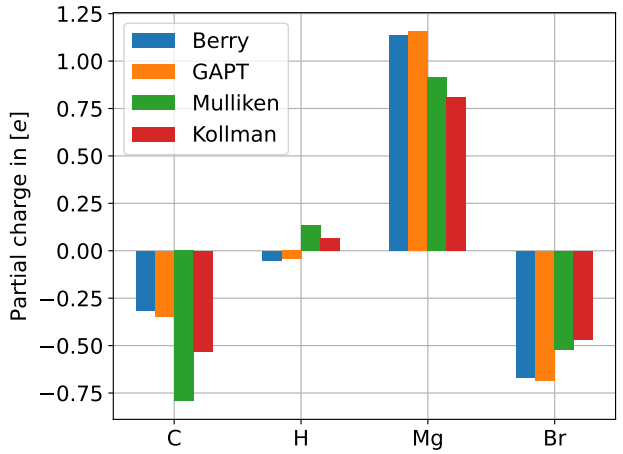

FIG. 6. Visualization of the partial charges in [e] for CH_3MgBr presented in table IX.

VI. CONCLUSION

The molecular Berry curvature plays a crucial role for quantum chemical calculations of molecules in finite magnetic fields. Due to its intimate connection to the motion of effective charges, recent years have even seen the emergence of a population analysis based on the Berry curvature.[24] While the close connection between the resulting Berry charges and charges based on the generalized atomic polar tensor (GAPT) were noticed in the literature, it remained somewhat elusive. In this work, we have derived a novel translational sum rule based on the electronic pseudomomentum for the molecular Berry curvature. Through this sum rule, we were able to reveal a deeper insight into the properties of the molecular Berry curvature, making an exact formulation of the connection between Berry and GAPT charges possible.

Furthermore, we have introduced a new algorithm capable of efficiently evaluating the molecular Berry curvature as well as other related response properties such as the atomic polar tensor for molecules in finite magnetic fields. Our algorithm is entirely integral-direct, avoiding the unfavorable transformation of the four-center two-electron integrals from the atomic orbital to the molecular orbital basis. This new algorithm was implemented into the TURBOMOLE program suite, where it will be available in the next official release version (V7.9).

Using the novel pseudomomentum-translational sum rule and our efficient implementation of the molecular Berry curvature, we have investigated the connection between Berry and GAPT charges. We were able to derive that both types of population analysis are equivalent in the limit of a complete basis set, which was also confirmed numerically. Finally, we demonstrated that Berry charges are often not a suitable choice of population analysis, exhibiting deficiencies that have already been described for the closely related GAPT charges in the literature. For instance, we could show that Berry charges are not suited to yield accurate descriptions for molecular properties such as the electric dipole moment. For the prediction of partial charges, they also yield relatively large differences to other models such as an electrostatic potential fit based on Kollman's parametrization. While the molecular Berry curvature remains a very important quantity for the description of molecular motion in an external magnetic field, Berry charges should only be used with great caution when trying to gain insight into the electronic structure of molecules.

SUPPORTING INFORMATION

The supporting information contains the molecular coordinates (xyz format) for all molecules discussed in this work. Furthermore, the molecular Berry curvature and the related atomic tensors are listed. This includes the geometry gradients of the electric dipole moment, the canonical momentum, and the electronic pseudomomentum.

DATA AVAILABILITY STATEMENT

The data that support the findings of this study are available within the article and its supplementary material.

ACKNOWLEDGMENTS

The authors would like to thank Wim Klopper, Maximilian Kronenberger, Laurenz Monzel, and Angela Bihlmeier for helpful discussions. D.S. gratefully acknowledges support by the Deutsche Forschungsgemeinschaft (DFG, German Research Foundation) via project Q of the CRC 1573 (4f for Future). A.P. gratefully acknowledges support from the Walter Benjamin Programme funded by the Deutsche Forschungsgemeinschaft (DFG, German Research Foundation) through DFG-529675149.

AUTHOR CONTRIBUTIONS AND DECLARATIONS

Dominik Steinmetz: Conceptualization (supporting); Data curation (lead); Formal analysis (equal); Investigation (equal); Methodology (equal); Software (equal); Validation (equal); Visualization (equal); Writing – original draft (equal); Writing – review & editing (equal).

Ansgar Pausch: Conceptualization (lead); Data curation (supporting); Formal analysis (equal); Investigation (equal); Methodology (equal); Software (equal); Validation (equal);

Visualization (equal); Writing – original draft (equal); Writing – review & editing (equal).

Notes

The authors declare no competing financial interest.

REFERENCES

[1] M. V. Berry, Proc. R. Soc. Lond. **392**, 45 (1984).
[2] C. A. Mead, Rev. Mod. Phys. **64**, 51 (1992).
[3] R. Resta, J. Phys. Condens. Matter **12**, R107 (2000).
[4] C. A. Mead and D. G. Truhlar, J. Chem. Phys. **70**, 2284 (1979).
[5] D. Ceresoli and E. Tosatti, Phys. Rev. Lett. **89**, 116402 (2002).
[6] S. Matsika and P. Krause, Annu. Rev. Phys. Chem. **62**, 621 (2011).
[7] M. H. Farag, A. Mandal, and P. Huo, Phys. Chem. Chem. Phys. **23**, 16868 (2021).
[8] Y. Aharonov and D. Bohm, Phys. Rev. **115**, 485 (1959).
[9] B. Göhler, V. Hamelbeck, T. Z. Markus, M. Kettner, G. F. Hanne, Z. Vager, R. Naaman, and H. Zacharias, Science **331**, 894 (2011).
[10] H.-H. Teh, W. Dou, and J. E. Subotnik, Phys. Rev. B. **106** (2022).
[11] X. Bian, T. Qiu, J. Chen, and J. E. Subotnik, J. Chem. Phys. **156**, 234107 (2022).
[12] P. Schmelcher, L. S. Cederbaum, and H. Meyer, Phys. Rev. A **38**, 6066 (1988).
[13] P. Schmelcher and L. S. Cederbaum, Phys. Rev. A **40**, 3515 (1989).
[14] L. Yin and C. A. Mead, Theoret. Chim. Acta **82**, 397 (1992).
[15] J. Peternelj and T. Kranjc, Z. Physik B - Condensed Matter **92**, 61 (1993).
[16] L. Yin and C. Alden Mead, J. Chem. Phys. **100**, 8125 (1994).
[17] P. Schmelcher and L. S. Cederbaum, Int. J. Quantum Chem. **64**, 501 (1997).
[18] T. Culpitt, L. D. M. Peters, E. I. Tellgren, and T. Helgaker, J. Chem. Phys. **155**, 024104 (2021).
[19] L. D. M. Peters, T. Culpitt, L. Monzel, E. I. Tellgren, and T. Helgaker, J. Chem. Phys. **155**, 024105 (2021).
[20] L. Monzel, A. Pausch, L. D. M. Peters, E. I. Tellgren, T. Helgaker, and W. Klopper, J. Chem. Phys. **157**, 054106 (2022).
[21] L. D. M. Peters, E. I. Tellgren, and T. Helgaker, Mol. Phys. **122** (2024).
[22] E. I. Tellgren, T. Culpitt, L. D. M. Peters, and T. Helgaker, J. Chem. Phys. **158**, 124124 (2023).
[23] T. Culpitt, L. D. M. Peters, E. I. Tellgren, and T. Helgaker, J. Chem. Phys. **158**, 114115 (2023).
[24] L. D. M. Peters, T. Culpitt, E. I. Tellgren, and T. Helgaker, J. Chem. Theory Comput. **19**, 1231 (2023).
[25] A. Pausch, "*Development and Application of Efficient Computational Methods for Molecular Spectroscopy in Finite Magnetic Fields*, phd thesis," (2022).
[26] T. Culpitt, L. D. M. Peters, E. I. Tellgren, and T. Helgaker, J. Chem. Phys. **156**, 044121 (2022).
[27] L. D. M. Peters, T. Culpitt, E. I. Tellgren, and T. Helgaker, J. Chem. Phys. **157**, 134108 (2022).
[28] R. S. Mulliken, J. Chem. Phys. **23**, 1833 (1955).
[29] R. S. Mulliken, J. Chem. Phys. **23**, 1841 (1955).
[30] R. S. Mulliken, J. Chem. Phys. **23**, 2338 (1955).
[31] P.-O. Löwdin, J. Chem. Phys. **18**, 365 (1950).
[32] E. N. Maslen and M. A. Spackman, Aust. J. Phys. **38**, 273 (1985).
[33] F. L. Hirshfeld, Theoret. Chim. Acta **44**, 129 (1977).
[34] U. C. Singh and P. A. Kollman, J. Comput. Chem. **5**, 129 (1984).
[35] J. Cioslowski, J. Am. Chem. Soc. **111**, 8333 (1989).
[36] A. Milani and C. Castiglioni, J. Mol. Struct. THEOCHEM **955**, 158 (2010).
[37] R. Ahlrichs, M. Bär, M. Häser, H. Horn, and C. Kölmel, Chem. Phys. Lett. **162**, 165 (1989).
[38] S. G. Balasubramani, G. P. Chen, S. Coriani, M. Diedenhofen, M. S. Frank, Y. J. Franzke, F. Furche, R. Grotjahn, M. E. Harding, C. Hättig, A. Hellweg, B. Helmich-Paris, C. Holzer, U. Huniar, M. Kaupp, A. Marefat Khah, S. Karbalaei Khani, T. Müller, F. Mack, B. D. Nguyen, S. M. Parker, E. Perlt, D. Rappoport, K. Reiter, S. Roy, M. Rückert, G. Schmitz, M. Sierka, E. Tapavicza, D. P. Tew, C. van Wüllen, V. K. Voora, F. Weigend, A. Wodyński, and J. M. Yu, J. Chem. Phys. **152**, 184107 (2020).
[39] Y. J. Franzke, C. Holzer, J. H. Andersen, T. Begušić, F. Bruder, S. Coriani, F. Della Sala, E. Fabiano, D. A. Fedotov, S. Fürst, S. Gillhuber, R. Grotjahn, M. Kaupp, M. Kehry, M. Krstić, F. Mack, S. Majumdar, B. D. Nguyen, S. M. Parker, F. Pauly, A. Pausch, E. Perlt, G. S. Phun, A. Rajabi, D. Rappoport, B. Samal, T. Schrader, M. Sharma, E. Tapavicza, R. S. Treß, V. Voora, A. Wodyński, J. M. Yu, B. Zerulla, F. Furche, C. Hättig, M. Sierka, D. P. Tew, and F. Weigend, J. Chem. Theory Comput. **19**, 6859 (2023).
[40] E. I. Tellgren, A. Soncini, and T. Helgaker, J. Chem. Phys. **129**, 154114 (2008).
[41] F. London, J. Phys. Radium **8**, 397 (1937).
[42] R. Ditchfield, Mol. Phys. **27**, 789 (1974).
[43] A. Pausch and W. Klopper, Mol. Phys. **118**, e1736675 (2020).
[44] C. Holzer, A. Pausch, and W. Klopper, Front. Chem. **9**, 746162 (2021).
[45] A. Pausch and C. Holzer, J. Phys. Chem. Lett. **13**, 4335 (2022).
[46] A. Pausch, C. Holzer, and W. Klopper, J. Chem. Theory Comput. **18**, 3747 (2022).
[47] S. Blaschke, S. Stopkowicz, and A. Pausch, J. Chem. Phys. **161** (2024).
[48] E. I. Tellgren, T. Helgaker, A. Soncini, K. K. Lange, A. M. Teale, U. Ekström, S. Stopkowicz, J. H. Austad, and S. Sen, "London, a quantum-chemistry program for plane-wave/gto hybrid basis sets and finite magnetic field calculations. see londonprogram.org for more information.".
[49] S. Sen, K. K. Lange, and E. I. Tellgren, J. Chem. Theory Comput. **15**, 3974 (2019).
[50] D. B. Williams-Young, A. Petrone, S. Sun, T. F. Stetina, P. Lestrange, C. E. Hoyer, D. R. Nascimento, L. Koulias, A. Wildman, J. Kasper, J. J. Goings, F. Ding, A. E. DePrince, III, E. F. Valeev, and X. Li, Wiley Interdiscip. Rev. Comput. Mol. Sci. **10** (2020).
[51] S. Sun, D. B. Williams-Young, T. F. Stetina, and X. Li, J. Chem. Theory Comput. **15**, 348 (2019).
[52] S. Sun, D. Williams-Young, and X. Li, J. Chem. Theory Comput. **15**, 3162 (2019).
[53] F. Hampe, S. Stopkowicz, N. Groß, M.-P. Kitsaras, L. Grazioli, S. Blaschke, L. Monzel, and Ü. P. Yergün, "Qcumbre, quantum chemical utility enabling magnetic-field dependent investigations benefitting from rigorous electron-correlation treatment. qcumbre.org,".
[54] F. Hampe and S. Stopkowicz, J. Chem. Phys. **146**, 154105 (2017).
[55] M.-P. Kitsaras, L. Grazioli, and S. Stopkowicz, J. Chem. Phys. **160** (2024).
[56] T. Shiozaki, Wiley Interdiscip. Rev. Comput. Mol. Sci. **8**, e1331 (2018).
[57] R. D. Reynolds and T. Shiozaki, Phys. Chem. Chem. Phys. **17**, 14280 (2015).
[58] "Quest, a rapid development platform for quantum electronic structure techniques. quest.codes, 2017,".
[59] M. Wibowo-Teale, B. J. Ennifer, and A. M. Wibowo-Teale, J. Chem. Phys. **159** (2023).
[60] B. S. Ofstad, M. Wibowo-Teale, H. E. Kristiansen, E. Aurbakken, M. P. Kitsaras, Ø. S. Schøyen, E. Hauge, T. J. P. Irons, S. Kvaal, S. Stopkowicz, A. M. Wibowo-Teale, and T. B. Pedersen, J. Chem. Phys. **159** (2023).
[61] M. Frisch, M. Head-Gordon, and J. Pople, Chem. Phys. **141**, 189 (1990).
[62] P. Deglmann, F. Furche, and R. Ahlrichs, Chem. Phys. Lett. **362**, 511 (2002).
[63] M. Gradhand, D. V. Fedorov, F. Pientka, P. Zahn, I. Mertig, and B. L. Györffy, Phys. Rev. B Condens. Matter Mater. Phys. **84** (2011).
[64] H.-H. Teh, W. Dou, and J. E. Subotnik, Phys. Rev. B. **104** (2021).
[65] P. Schmelcher and L. S. Cederbaum, Phys. Rev. A **37**, 672 (1988).
[66] M. Gell-Mann, Nuovo Cimento **4**, 848 (1956).
[67] G. Vignale and M. Rasolt, Phys. Rev. Lett. **59**, 2360 (1987).
[68] G. Vignale and M. Rasolt, Phys. Rev. B Condens. Matter **37**, 10685 (1988).
[69] M. E. Casida, Comput. Theor. Chem. **914**, 3 (2009).
[70] J. P. Perdew, K. Burke, and M. Ernzerhof, Phys. Rev. Lett. **77**, 3865 (1996).
[71] F. Weigend and R. Ahlrichs, Phys. Chem. Chem. Phys. **7**, 3297 (2005).
[72] O. Treutler and R. Ahlrichs, J. Chem. Phys. **102**, 346 (1995).
[73] F. Weigend, Phys. Chem. Chem. Phys. **8**, 1057 (2006).
[74] A. Pausch, M. Gebele, and W. Klopper, J. Chem. Phys. **155** (2021).
[75] T. J. Barton, R. W. Roth, and J. G. Verkade, J. Am. Chem. Soc. **94**, 8854 (1972).
[76] U. Dinur and A. T. Hagler, J. Chem. Phys. **91**, 2949 (1989).
[77] A. Milani and C. Castiglioni, J. Phys. Chem. A **114**, 624 (2010).

[78]F. T. Prochaska and L. Andrews, J. Am. Chem. Soc. **100**, 2102 (1978).
[79]G. A. Olah, G. Rasul, A. K. Yudin, A. Burrichter, G. K. Surya Prakash, A. L. Chistyakov, I. V. Stankevich, I. S. Akhrem, N. P. Gambaryan, and M. E. Vol'pin, J. Am. Chem. Soc. **118**, 1446 (1996).
[80]I. Krossing, A. Bihlmeier, I. Raabe, and N. Trapp, Angew. Chem. Int. Ed. **42**, 1531 (2003).
[81]H. P. A. Mercier, M. D. Moran, G. J. Schrobilgen, C. Steinberg, and R. J. Suontamo, J. Am. Chem. Soc. **126**, 5533 (2004).